










ESCRT components ISTL1 and LIP5 are required for tapetal function and pollen viability

Kaija Goodman ^{1,2} Julio Paez-Valencia ^{1,2} Janice Pennington ^{1,2,3} Annika Sonntag ⁴
 Xinxin Ding ^{1,2} Han Nim Lee ^{1,2} Paul G. Ahlquist ^{3,5,6,7} Isabel Molina ⁴ and
 Marisa S. Otegui ^{1,2,*†}

- 1 Department of Botany, University of Wisconsin-Madison, Wisconsin 53706, USA
- 2 Center for Quantitative Cell Imaging, University of Wisconsin-Madison, Madison, Wisconsin 53706, USA
- 3 Institute for Molecular Virology, University of Wisconsin-Madison, Madison, Wisconsin 53706, USA
- 4 Department of Biology, Algoma University, Ontario P6A 2G4, Canada
- 5 Department of Oncology and Plant Pathology, University of Wisconsin-Madison, Madison, Wisconsin 53706, USA
- 6 Howard Hughes Medical Institute, Chevy Chase, Maryland 20815, USA
- 7 Morgridge Institute for Research, Madison, Wisconsin 53706, USA

*Author for Correspondence: otegui@wisc.edu

†Senior author.

K.G. analyzed *istl1 lip5* fertility defects, generated fluorescent marker lines, and performed confocal and scanning electron microscopies. M.S.O., J.P., and K.G. performed transmission electron microscopy and tomography. X.D. analyzed the expression data and collected the imaging data. X.D. and H.-N.L. isolated transgenic lines. J. P.-V. performed the pollen viability assays. A.S. and I.M. performed the anther wax analysis. P.G.A. interpreted results and provided critical resources and expertise for the electron microscopic studies. K.G. and M.S.O. wrote the manuscript with contributions and feedback from all other coauthors.

The author responsible for distribution of materials integral to the findings presented in this article in accordance with the policy described in the Instructions for Authors (<https://academic.oup.com/plcell>) is: Marisa S. Otegui (otegui@wisc.edu).

Abstract

Pollen wall assembly is crucial for pollen development and plant fertility. The durable biopolymer sporopollenin and the constituents of the tryphine coat are delivered to developing pollen grains by the highly coordinated secretory activity of the surrounding tapetal cells. The role of membrane trafficking in this process, however, is largely unknown. In this study, we used *Arabidopsis thaliana* to characterize the role of two late-acting endosomal sorting complex required for transport (ESCRT) components, ISTL1 and LIP5, in tapetal function. Plants lacking ISTL1 and LIP5 form pollen with aberrant exine patterns, leading to partial pollen lethality. We found that ISTL1 and LIP5 are required for exocytosis of plasma membrane and secreted proteins in the tapetal cells at the free microspore stage, contributing to pollen wall development and tryphine deposition. Whereas the ESCRT machinery is well known for its role in endosomal trafficking, the function of ISTL1 and LIP5 in exocytosis is not a typical ESCRT function. The *istl1 lip5* double mutants also show reduced intraluminal vesicle concatenation in multivesicular endosomes in both tapetal cells and developing pollen grains as well as morphological defects in early endosomes/trans-Golgi networks, suggesting that late ESCRT components function in the early endosomal pathway and exocytosis.

IN A NUTSHELL

Background: The development of pollen grains in flowering plants requires the participation of a secretory tissue called the tapetum within the anther. Through its secretory activity, the tapetum is essential for the formation of the complex pollen wall. This tapetal function is mediated by both the activity of transporters at the plasma membrane and the release into the anther locule of proteins and other molecules packed in secretory vesicles. The tapetum only lives for 4 days in *Arabidopsis*, and we know very little about how its intense secretory activity is regulated during this period of time.

Question: We wanted to know how the proteins LIP5 and ISTL1, which are known to mediate internalization and degradation of plasma membrane proteins in other plant cells types and organisms, regulate the secretory activity of the tapetum in *Arabidopsis*.

Findings: *Arabidopsis* mutant plants that lack both LIP5 and ISTL1 function produce abnormal pollen grains due to defective tapetal secretion. Unexpectedly, we found that these proteins not only regulate the degradation of plasma membrane proteins but also their delivery to the surface of tapetal cells (exocytosis) during the formation of pollen grains. This double mutation also causes structural defects in the endosomes of tapetal cells.

Next steps: We are working now to understand why tapetal cells are particularly sensitive to mutations in the *LIP5* and *ISTL1* genes and how these two proteins mediate exocytosis.

Introduction

Tapetal cells are one of the most fascinating yet least understood cell types in flowering plants. They line the locule of the anther and provide microspores and pollen grains with metabolites, nutrients, and critical molecules for the assembly of the pollen wall (Pacini et al., 1985). In *Arabidopsis thaliana*, the tapetum secretes metabolites into the locule and remains functional for only 4 days (Smyth et al., 1990; Sanders et al., 1999), but without it, pollen grains fail to develop, resulting in male sterility. Tapetal cells become binuclear and polyploid by restitution mitosis (i.e. binucleate cells enter mitosis but all the chromosomes share a single metaphase plate, resulting in a cell with two nuclei with duplicated sets of chromosomes (Valuchova et al., 2020) before undergoing programmed cell death during late stages of pollen development. Right after microspore mother cells undergo meiosis, the tapetum secretes callases that degrade the callose encasing the tetrad, allowing for the release of the individual haploid microspores (Zhang et al., 2007). The tapetal cells then synthesize precursor molecules for the assembly of sporopollenin, one of the toughest and most durable polymers in nature. Sporopollenin forms the outer layer of the pollen grain or exine and is resistant to fossilization (Brooks and Shaw, 1968). Finally, during later stages, the tapetum synthesizes sterol esters, waxes, flavonoids, and proteins that fill the cavities and crevices of the exine forming the tryphine (or pollen coat), which acts as a chemical and physical interface between the pollen grain and its environment and is critical for protection against UV (ultraviolet) radiation, insect-mediated pollination, and pollen hydration at the stigma (Shi et al., 2015). In *Arabidopsis* and other Brassicaceae, flavonoids and alkanes are stored in a tapetum-specific organelle called the tapetosome (Hsieh and Huang, 2007), which is derived from the endoplasmic

reticulum (ER), whereas sterol esters accumulate in modified plastids called elaioplasts (Wu et al., 1999).

Although many of the enzymes responsible for the synthesis of these highly specialized metabolites are known (no other cell type in land plants synthesizes sporopollenin precursors), how exactly these metabolites are trafficked within tapetal cells and secreted into the locule is less clear. The completion of programmed cell death leads to tapetum breakdown and the release of all its cellular contents, including tapetosomes and elaioplasts, into the locule. However, prior to this last step, materials targeted to the anther locule are exported through the plasma membrane, employing both exocytosis and plasma membrane transporters. In fact, tapetal cells are devoid of cell walls; instead their plasma membranes make contact with the locule to facilitate the massive export of metabolites (Quilichini et al., 2014a).

Several plasma membrane transporters, including some ATP-binding cassette (ABC) transporters of the G subfamily, have been implicated in metabolite export from the tapetum into the anther locule. *Arabidopsis* ABCG26 transports polyketide sporopollenin precursors for exine formation (Quilichini et al., 2010, 2014b; Choi et al., 2011; Dou et al., 2011; Kuromori et al., 2011). The secretion of tryphine components seems to involve several transporters. ABCG9 and ABCG31 mediate export of sterol glycosides (Choi et al., 2014), whereas the transporter NPF2.8 seems to facilitate the release of flavonol sophorosides into the anther locule (Grunewald et al., 2020). ABCG1 and ABCG16 are also required for pollen development, but the nature of their substrates is unclear (Yadav et al., 2014).

Exocytosis is also required for tapetal function. Seed plant-specific type III lipid transfer proteins or LTPs that are exclusively expressed in the tapetum are trafficked from the ER to the trans-Golgi network (TGN), either bound or unbound

to sporopollenin precursors, and are exported into the locule by exocytosis to become incorporated into the pollen exine (Huang et al., 2013). Thus, during its short life, the tapetum changes its biosynthetic and secretory activities drastically to accommodate the demands of the microspores and pollen grains. Therefore, it is logical to predict that tapetal cells require very tight regulation of their endomembrane secretory system and plasma membrane composition to ensure the sequential secretory phases of the tapetum.

Selective degradation of plasma membrane proteins, such as transporters, is mediated by endocytosis and endosomal sorting for vacuolar degradation. Plasma membrane proteins (cargo) are tagged for degradation by ubiquitination and are internalized into endocytic vesicles that are transported to early endosomes, which in plants correspond to the TGN (Dettmer et al., 2006; Lam et al., 2008). Cargo can be deubiquitinated and recycled back to the plasma membrane or remain in the endosomal system to be sequestered into intraluminal vesicles of multivesicular endosomes (MVEs). Upon maturation, MVEs fuse with vacuoles/lysosomes, releasing cargo-loaded intraluminal vesicles, which are degraded by the action of local hydrolases (Luzio et al., 2014; Paez Valencia et al., 2016).

The recognition of ubiquitinated cargo proteins and their sequestration into endosomal vesicles are mediated by the endosomal sorting complex required for transport (ESCRT) machinery. The canonical ESCRT machinery in the Opisthokonta clade consists of ESCRT-0, ESCRT-I, ESCRT-II, ESCRT-III, and the SKD1 (Suppressor of K⁺ Transport Growth Defect 1; known as VPS4 in mammals and fungi)–LIP5 (Lyst-Interacting Protein 5; also known as Vta1p in fungi) complex, which are sequentially recruited during endosomal sorting and intraluminal vesicle formation. Lineages lacking ESCRT-0, including plants, instead utilize the more ancestral TOM1 and TOM1-like (TOL) proteins to recognize ubiquitinated cargo (Korbei et al., 2013; Moulinier-Anzola et al., 2020). Early acting ESCRTs, such as ESCRT-0/TOLs, ESCRT-I, and ESCRT-II, contain ubiquitin-binding domains that interact with ubiquitinated cargo to cluster them to sites of forming vesicles and initiate membrane bending (Katzmann et al., 2001; Wollert and Hurley, 2010; Schuh and Audhya, 2014). ESCRT-III subunits do not interact with ubiquitin but form heterogeneous filamentous spirals around the clustered cargo to deform the membrane, constricting the neck of the nascent vesicle (Hanson et al., 2008; Fyfe et al., 2011; Shen et al., 2014; Chiaruttini et al., 2015; Pfitzner et al., 2020). The AAA ATPase SKD1 and its positive regulator LIP5 bind and remodel the ESCRT-III spirals (Shen et al., 2014; Mierzwa et al., 2017; Maity et al., 2019), facilitating vesicle release into the endosomal lumen. However, the exact mechanism is not entirely clear.

In plants, endosomal intraluminal vesicles do not form individually but rather, vesicles are formed as concatenated networks and internalize ESCRT-III, which stabilizes inter-vesicle bridges (Buono et al., 2017). Regardless of how SKD1 mediates vesicle formation, it is an essential component of the ESCRT machinery and for Arabidopsis, indispensable for

development and cell viability (Haas et al., 2007; Shahriari et al., 2010). Not surprisingly given its essential role, SKD1 activity is tightly regulated by a variety of factors. LIP5 (also called Vta1p in yeast) increases SKD1 ATPase activity in vitro (Haas et al., 2007; Azmi et al., 2008; Rue et al., 2008). In addition, the plant-specific ESCRT protein Positive Regulator of SKD1 enhances the activity of SKD1 in vitro (Reyes et al., 2014). Other proteins such as the ESCRT-III accessory subunits CHMP1, VPS60, and IST1 modulate the recruitment of SKD1 to endosomal membranes (Azmi et al., 2008; Dimaano et al., 2008; Nickerson et al., 2010). More specifically, yeast Ist1p has been reported to play both negative and positive roles in SKD1 activity (Dimaano et al., 2008; Jones et al., 2012; Tan et al., 2015; Buono et al., 2016; Frankel et al., 2017). In yeast, Ist1p regulates Vps4p in a dose-dependent manner and therefore uniquely modulates the endosomal pathway. At low concentrations, Ist1p increases Vps4p activity by stimulating the recruitment of Vps4p to endosomal membranes, whereas at high concentrations, Ist1p directly binds to Vps4p, inhibiting both its ATPase activity and its interaction with other ESCRTs (Dimaano et al., 2008; Jones et al., 2012; Tan et al., 2015).

In Arabidopsis, there are 12 IST1-LIKE (ISTL) proteins, of which ISTL1 plays the role of a canonical IST1 subunit in endosomal sorting (Buono et al., 2016). As is typical for IST1 in other organisms, Arabidopsis ISTL1 physically and genetically interacts with LIP5 (Dimaano et al., 2008; Rue et al., 2008; Buono et al., 2016). Whereas lack of IST1 function in the nematode *Caenorhabditis elegans* causes plasma membrane protein mis-sorting and the formation of MVEs with smaller intraluminal vesicles (Frankel et al., 2017), yeast and Arabidopsis mutants for *Ist1* and *ISTL1*, respectively, do not exhibit detectable abnormalities in endosomal sorting or physiological responses under normal growth conditions. Arabidopsis *lip5* mutants show slightly reduced growth due to impaired cell expansion, reduced responses to abscisic acid, and compromised tolerance to heat, drought, salt stress, and bacterial pathogens (Haas et al., 2007; Xia et al., 2013, 2016; Wang et al., 2014, 2015; Buono et al., 2016). However, eliminating both ISTL1 and LIP5 functions results in severely dwarf plants with constitutively upregulated biotic defense responses and impaired fertility (Buono et al., 2016).

Given the predicted central role of plasma membrane protein homeostasis and endomembrane trafficking in the tapetal cells of Arabidopsis, we investigated the role of two ESCRT components, ISTL1 and LIP5, in tapetal function. We found that LIP5 and ISTL1 are required for the exocytosis of the plasma membrane ABCG9 transporter and secretion of a type III LTP, specifically during the free microspore stage. The exocytic trafficking of these cargo proteins is critical for pollen wall development but is not a typical ESCRT function. In addition, the *istl1 lip5* double mutants not only show drastic structural defects in MVEs, including reduced intraluminal vesicle concatenation, in tapetal cells and developing pollen grains but also morphological disruptions of early endosomes/TGN, bringing important insights into the

potential roles of late ESCRT components in the early endosomal pathway and exocytosis.

Results

ISTL1 and LIP5 are required for gametophyte and seed development

The *istl1-1 lip5-1* double mutant plants exhibit dwarfism due to reduced cell expansion, early senescence, and constitutive defense response, as evidenced by the upregulated expression of the defense response marker gene *PR1* (*PATHOGEN-RELATED1*), even in the absence of pathogens or their elicitors (Buono et al., 2016). Similar to other mutants showing constitutive defense response, *istl1 lip5* mutant plants kept at high temperature (28°C) are able to grow and enter the reproductive phase. However, although able to form flowers, *istl1 lip5* plants at 28°C fail to develop seeds, suggesting that infertility is directly connected to defective ESCRT function and not to the constitutive defense response.

To investigate the role of ISTL1 and LIP5 in fertility, we analyzed pollen viability in *istl1 lip5* anthers by Alexander's staining, which results in viable pollen grain turning magenta and aborted pollen, blue-green (Alexander, 1969; Peterson et al., 2010). Whereas wild-type (WT), single, and *istl1-1 lip5-1/+* mutants contained on average 2%–3% of aborted pollen grains in their anthers, a much higher (up to 40%) and more variable proportion of aborted pollen was produced by *istl1 lip5* double homozygous mutant anthers in plants grown at 28°C (Figure 1, A and B).

To rule out potential deleterious effects of high temperatures on pollen development (Sakata et al., 2010; Dündar et al., 2019), we blocked the salicylic-dependent constitutive pathogen response in the *istl1 lip5* mutant by introducing the *sid2-2* mutation, which impairs salicylic acid synthesis (Wildermuth et al., 2001), and analyzed *istl1 lip5 sid2* triple mutant and control plants grown at 22°C. Like *istl1 lip5* plants grown at 28°C, the *istl1 lip5 sid2* triple mutant grown at 22°C produced flowers with an abnormally high proportion of aborted pollen grains (Supplemental Figure S1) and a reduced seed set, suggesting that the defective fertility observed in the *istl1 lip5* double mutant is not a pleiotropic defect due to the activation of the constitutive pathogen response but most likely, a direct result of impaired ISTL1 and LIP5 functions.

To analyze whether *istl1 lip5* pollen grains were able to lead to successful fertilization and seed formation, we performed a pollination competition assay, wherein we hand-pollinated the stigma of a WT Col-0 flower with pollen from an *istl1-1 lip5 +/-* plant. As shown previously, these plants carrying one WT allele of *LIP5* produce viable pollen grains (Figure 1, A and B). Whereas all pollen grains should carry the *istl1* mutant allele, 50% of them should also carry the *lip5* mutation. If the double *istl1 lip5* mutant pollen grains are functional, pollination of a WT flower should result in 50% of the seed set carrying the *lip5* mutant allele. We found that 48.8% of the resulting seeds contained the *lip5* mutation (expected: 50%, observed: 48.8%, $n = 170$),

indicating that the combination of the *istl1* and *lip5* mutations per se does not affect pollen development and function. Consistently, when *istl1-1 lip5 +/-* plants were allowed to self-pollinate, they produced a normal seed set in which approximately one fourth of the resulting seeds were *istl1 lip5* double homozygous mutants (expected: 25%; observed: 25.2%; $n = 127$), as expected for normal transmission of the mutant alleles. These results, together with the normal proportion of viable pollen grains observed in *istl1-1 lip5 +/-* (Figure 1, A and B), suggest that the abortion of pollen grains in *istl1 lip5* homozygous mutant plants is due to maternal (sporophytic) defects.

Although only a portion of the pollen grains produced by *istl1 lip5* plants aborted during development, mutant plants were largely unable to produce seeds, suggesting that reduced pollen viability is not the only underlying cause for the reduced fertility of the *istl1 lip5* mutant. We analyzed mature siliques from *istl1 lip5 sid2* triple mutants that were either allowed to self-pollinate or pollinated with WT pollen (Figure 1, C–E). Both the *istl1 lip5 sid2* triple mutant and WT ovaries contained similar total numbers of ovules (mean = 43.2 per silique; Student's *t* test, $P = 0.16$, $n = 6$ WT, and 9 *istl1 lip5 sid2* siliques). However, compared to self-pollinated WT flowers in which we rarely observed unfertilized/aborted ovules (0.3%; $n = 6$ siliques), triple mutant siliques resulting from self-pollination showed an approximately 50% reduction in seed set due to unfertilized/aborted ovules (Figure 1, C and D). In addition, approximately 22% of the resulting seeds were arrested and shriveled (Figure 1, C and D). Whereas 60% of the ovules were fertilized and initiated seed development from *istl1 lip5 sid2* flowers manually pollinated with WT pollen (a slightly higher proportion compared to the self-pollinated siliques), 45% of them were shriveled and did not complete development (Figure 1D).

We then analyzed more carefully the shriveled seeds from self- and manually pollinated *istl1 lip5 sid2* mature siliques to identify at which developmental stage they were arrested. More than half of these seeds contained embryos at the torpedo or earlier stages, and approximately 22% of the seeds were arrested at the bent cotyledon embryo stage (Figure 1E). The mutant siliques derived from self-pollination but not the ones pollinated with WT pollen contained shriveled seeds with abnormal embryos (Figure 1, C and E). These results indicate that in addition to aborted pollen, a maternally derived defect in ovule development and abnormal seed development in *istl1 lip5* contributes to its reduced fertility.

ISTL1 and LIP5 are important for exine and tryphine deposition

Whereas many ESCRT components have been reported to affect different aspects of plant development, embryo morphogenesis, and biotic and abiotic responses (Spitzer et al., 2009; Isono et al., 2010; Katsiarimpa et al., 2011, 2013; Korbei et al., 2013; Spallek et al., 2013; Xia et al., 2013, 2016; Cai et

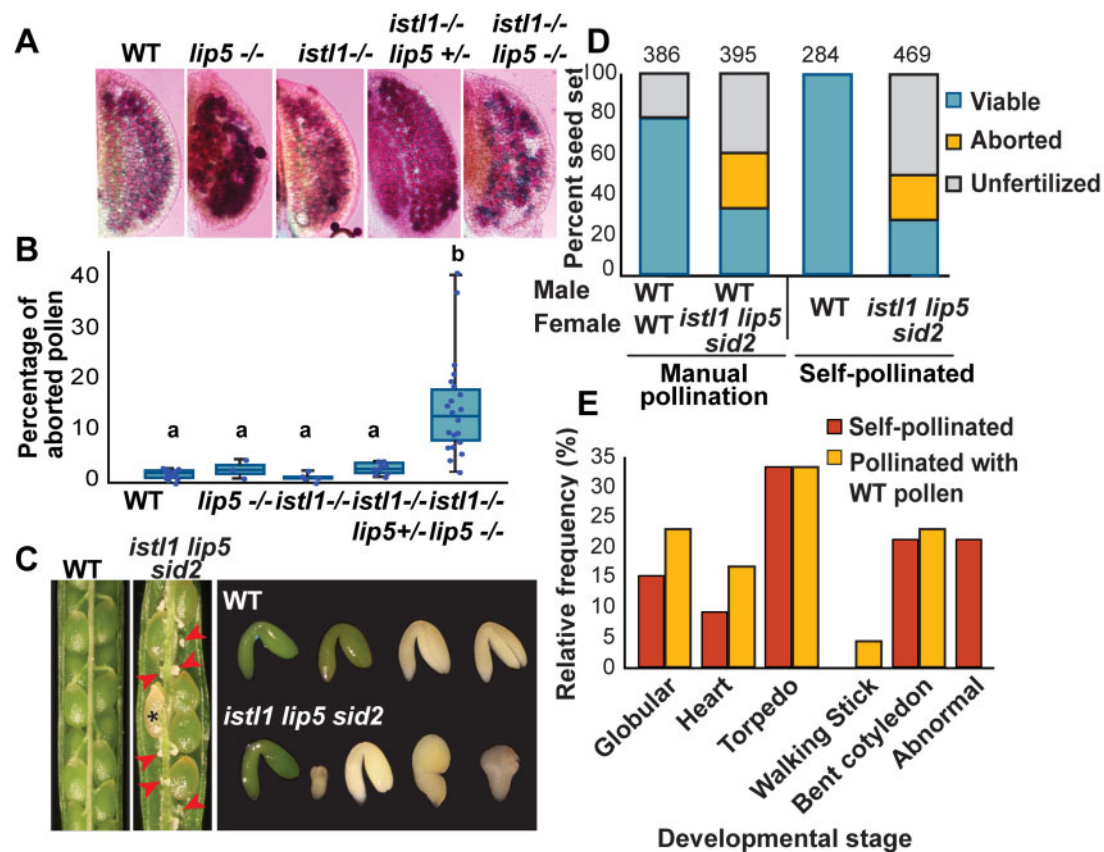


Figure 1 Fertility defects in *ist1 lip5* mutants. A, Detection of viable and aborted pollen by Alexander's staining in WT, single *ist1* and *lip5* mutants, *ist1* -/- *lip5* +/-, and homozygous *ist1 lip5* double mutant anthers from plants grown at 28°C. B, Quantification of aborted pollen grains from at least three anthers of each genotype ($n = 11$ WT, 3 *lip5*, 5 *ist1*, 6 *ist1* -/- *lip5* +/-, and 16 *ist1 lip5* anthers). The boxes show the 25th and 75th percentiles, middle lines indicate the median, and whiskers refer to upper and lower fences. Different letters represent significant differences (one-way ANOVA followed by Tukey, $P < 0.05$; See Supplemental File 1). C, Dissected mature siliques showing ovule (red arrowheads) and seed (asterisk) abortion in self-pollinated *ist1 lip5 sid2* plants ($n = 9$ siliques from manually pollinated WT; 9 siliques from WT manually pollinated triple mutants; 6 siliques from self-pollinated WT; and 12 siliques from self-pollinated triple mutant plants). Aborted seeds contained arrested or abnormal embryos. D, Analysis of seed set in manually and self-pollinated WT and *ist1 lip5 sid2* triple mutant plants. Numbers on top of each bar indicate the quantity of seeds analyzed. E, Quantification of developmental stages of arrested embryos in aborted seeds in *ist1 lip5 sid2* plants either self-pollinated ($n = 33$ embryos) or pollinated with WT pollen ($n = 48$ embryos).

al., 2014; Gao et al., 2014; Reyes et al., 2014; Wang et al., 2014, 2015; Cardona-López et al., 2015; Kalinowska et al., 2015; Kolb et al., 2015; Belda-Palazon et al., 2016; Buono et al., 2016; Liu et al., 2021), the *ist1 lip5* double mutant seems to be unique in having a drastic effect on gametophyte development. We focused our analysis in the development of pollen grains in the *lip5* and *ist1* single and *ist1 lip5* double mutants.

To understand why pollen viability is partially compromised in the *ist1 lip5* double mutant, we analyzed the morphology of the pollen cell wall in WT, *lip5* and *ist1* single and *ist1 lip5* double mutants by scanning electron microscopy. Mature *Arabidopsis* pollen grains are surrounded by three cell wall layers: the outer exine, the inner intine, and the tryphine filling the exine crevices. The exine consists of a foot layer or nexine, column-like structures called bacula, and the outermost tectum with a reticulate pattern. The scaffold of the future exine (called primexine) is formed by the microspore while still encased by the callosic wall of the

tetrad. Upon microspore release, the sporopollenin precursors secreted by the tapetum impregnate the primexine, forming the mature exine (Blackmore et al., 2007; Ariizumi and Toriyama, 2011). The intine is made of cellulose, pectins, and other polysaccharides and is assembled by the microspore.

Whereas 80%–90% of pollen grains from *ist1 lip5* mutant anthers showed normal reticulate patterns like those seen in WT, *lip5*, and *ist1* single mutant pollen grains or had slightly modified patterns with regions displaying larger or smaller lumina (gaps) or smooth patches, 10%–20% of the double mutant pollen showed only remnants of bacula or completely smooth surfaces (Figure 2, A and B).

To analyze in more detail the pollen cell wall defects, we imaged *ist1 lip5* double mutant mature pollen grains by transmission electron microscopy and electron tomography. Whereas the intine was normal in terms of thickness and texture, the exine layer in *ist1 lip5* double mutant pollen was much more variable in terms of thickness and

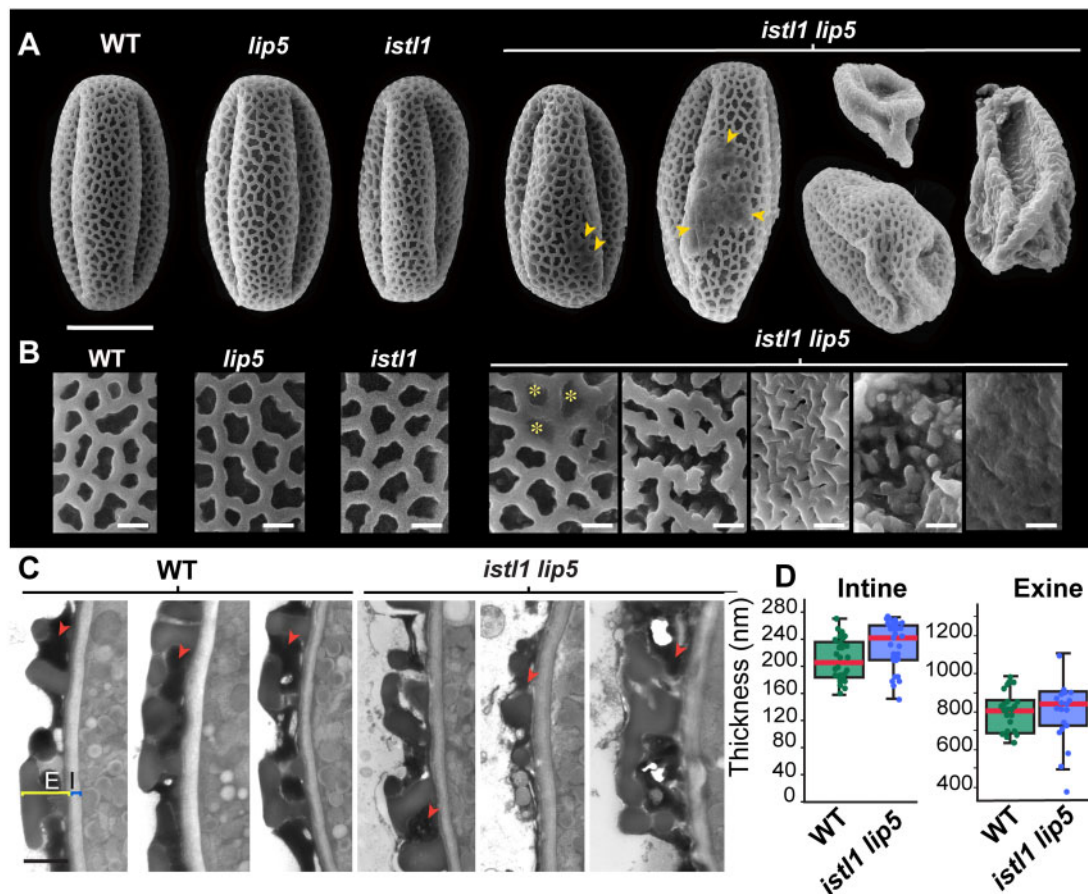


Figure 2 Pollen wall architecture. A and B, Scanning electron micrographs of WT, *istl1*, *lip5*, and *istl1 lip5* mature pollen released from mature anthers. Pollen from *istl1 lip5* display a range of defective exine morphologies. Arrowheads in (A) indicate abnormal patches of flattened exine and asterisks in (B), areas with covered gaps. C, Transmission electron micrographs of mature pollen grains showing exine (E), intine (I), and tryphine (arrowheads) in WT and *istl1 lip5* mutant pollen. D, Box and whisker plots show variation in exine and intine thickness in WT and *istl1 lip5* pollen. The boxes show the 25th and 75th percentiles, middle lines indicate the median, and whiskers refer to upper and lower fences. At least 10 pollen grains of each genotype were analyzed. Scale bars = 10 μm in (A); 1 μm in (B), and 800 nm in (C).

patterning compared to the WT (Figure 2, C and D), which is consistent with the results of our scanning electron microscopy image analysis. Lastly, although present in both WT and *istl1 lip5* double mutant pollen grains, the deposition pattern of tryphine seemed to be much more variable in the double mutant than in WT (Figure 2C).

We then investigated which step(s) in pollen development were affected in the *istl1 lip5* double mutant by analyzing developing anthers. The *istl1 lip5* mutant anthers developed free microspore and bicellular pollen grains that frequently (approximately 90% of the observed microspores/pollen grains) contained large concentric double-membrane structures of unknown origin that were not detected in WT anthers (Figure 3, A–E'). At the tri-cellular stage, between 30% and 40% of the *istl1 lip5* pollen grains were collapsed or highly vacuolated (Figure 3, F–L; Supplemental Figure S2).

Since our genetic and pollen viability analyses (Figure 1, A and B) indicated that the pollen developmental defects in the *istl1 lip5* double mutant were due to a maternal effect, we also analyzed the anther wall. In Arabidopsis, the anther wall consists of the epidermis, endothecium, middle layer,

and the tapetum in contact with the locule. In developing *istl1 lip5* mutant anthers, we did not observe structural alterations in any of the anther wall layers during the development of microspores and pollen grains (Supplemental Figure S3). More specifically, tapetal cells in both WT and mutant anthers developed normally and underwent programmed cell death by the time the pollen grains reached the late bicellular stage (Figure 3, F and H; Supplemental Figure S3). However, at this stage, we noticed an unusual occurrence of crystalline material reminiscent of waxes inside the locule of *istl1 lip5* double mutant anthers (Figure 3, K–M), indicative of abnormal tapetal activity and/or deficient incorporation into the pollen wall.

Analysis of wax composition

Some of the pollen wall defects seen in the double *istl1 lip5* mutant are consistent with the abnormal deposition of wax components within the tryphine. As the *istl1 lip5* mutant produces few seeds and flowers, we were unable to collect the large amount of pollen (e.g. 10 ng from 3,000 plants; Choi et al., 2014) required to analyze tryphine wax

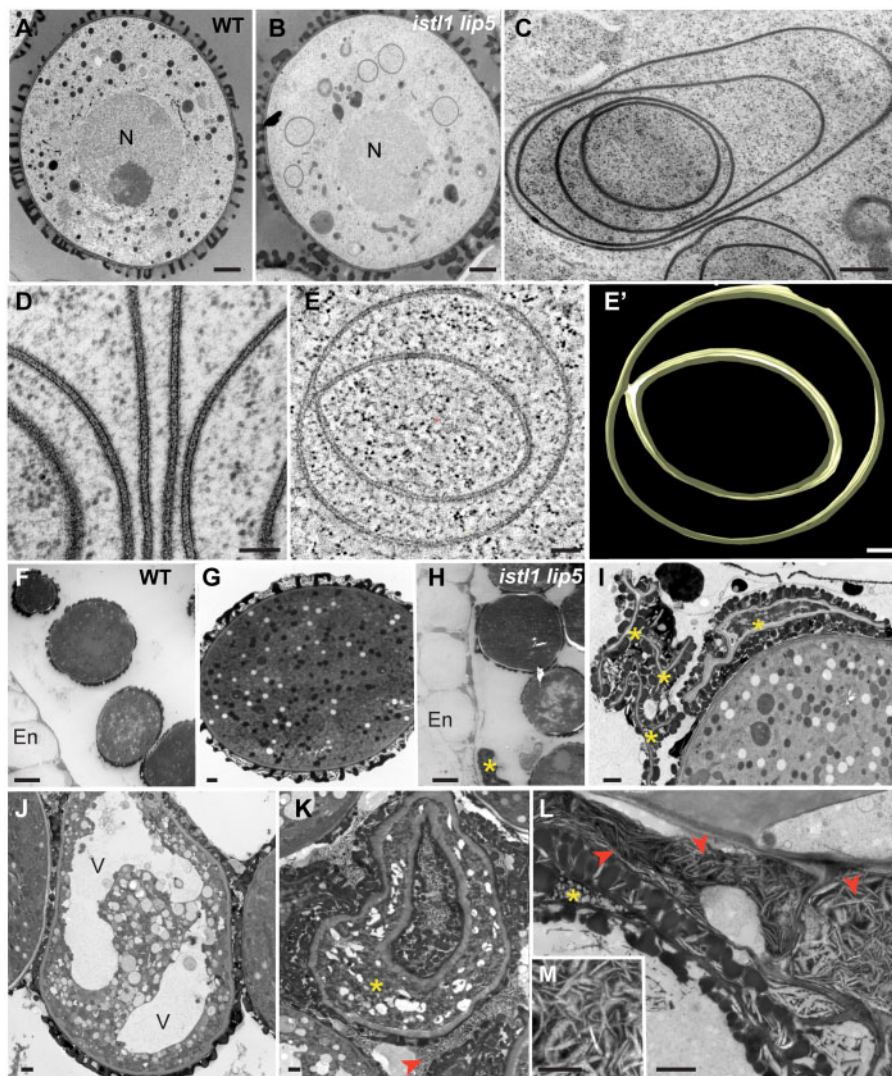


Figure 3 Ultrastructural features of microspores and pollen grains. A, WT and (B) *ist1 lip5* microspores prior to vacuolation. C and D, Most mutant microspores show large concentric double-membrane structures of unknown origin. (E) Electron tomographic slice and (E') corresponding tomographic reconstruction of a portion of a double-membrane structure. (F) The overview of mature WT pollen grains within a locule. G, WT pollen grains. H, The overview of mature pollen within an *ist1 lip5* anther with some collapsed grains (asterisk). I–L, Collapsed pollen grains (asterisks) in *ist1 lip5* anthers and highly vacuolated pollen (J) prior to collapse. Crystalline material was observed in *ist1 lip5* locules (red arrowheads in (K) and (L)). (M) Detail of crystalline material accumulated in the mutant anther locules. En, endothecium; N, nucleus; V, vacuole. Scale bars= 1 μ m in (A), (B), (G), (I), (J), (K), and (L); 400 nm in (C), 100 nm in (D), (E), and (E'); 6 μ m in (F) and (H); 500 nm in (M).

composition. Instead, we analyzed waxes in whole anthers of WT and single and double mutant flowers using gas chromatography coupled with mass spectrometry (GC–MS). Overall, we did not detect changes in any of the most abundant wax components, including free fatty acids (16:0 and 18:0) and the alkane nonacosane (C29:0), among WT and mutants (Figure 4). Among the less abundant alkanes, a reduction in the level of an isomer of triacontane (C30:0 iso) was detected in all single and double mutants, but this decrease was more pronounced in the *ist1 lip5* double mutant. The level of a hentriacontane isomer (C31:0 iso) was reduced in all mutant anthers, whereas hentriacontane (C31:0) levels were significantly reduced only in the *ist1 lip5* double mutant (Figure 4). Among sterols, which were also a minor component of whole anther waxes, β -sitosterol and

campesterol levels were reduced in single and double mutant anthers (Figure 4). These results indicate that all major wax components were not altered and that the accumulation of some minor alkane and sterol components was reduced in single and double mutant anthers. However, the reduced accumulation of some of these compounds is most likely not directly connected to the reduced pollen viability seen only in the *ist1 lip5* mutant but not in the corresponding single mutant anthers.

Endosomal structural features in tapetum and pollen

To determine the underlying cause for reduced pollen viability in the double *ist1 lip5* mutant, we analyzed the distribution and structural features of MVEs in both pollen and

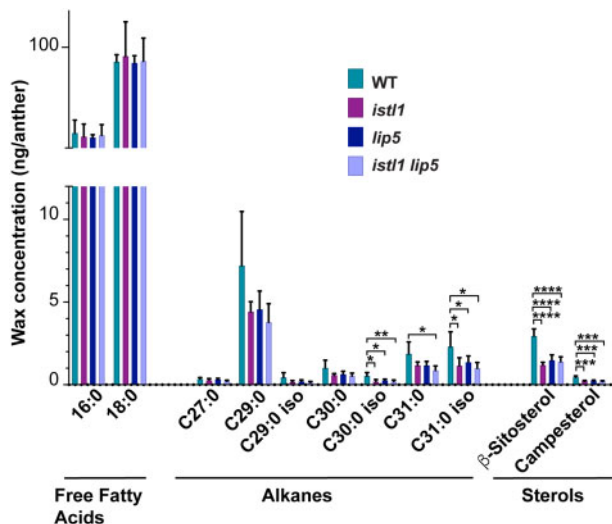


Figure 4 Analysis of anther waxes. Wax components extracted by rapid immersion in chloroform of lyophilized anthers were identified and quantified by GC–MS. Values are means from four biological replicates consisting of approximately 50 anthers each \pm s.d. Statistical analysis was performed with GraphPad Prism, using one-way ANOVA with Tukey’s multiple comparison posttest. Results were designated significant when the $P < 0.05$ (* $P < 0.05$; ** $P < 0.01$; *** $P < 0.001$, **** $P < 0.0001$; see Supplemental File 1).

tapetal cells in mutant anthers. We introduced RHA1/RabF2a-GFP (late endosome marker) and VHAa1-GFP (TGN marker) into *ist11 lip5* plants and analyzed the anthers by confocal microscopy. Based on the signal from these fluorescent markers, we did not observe differences in the distribution, abundance, or size of the TGN or MVEs between *ist11 lip5* and WT (Supplemental Figure S4).

We then imaged *ist11 lip5* anthers using transmission electron microscopy to analyze potential structural differences in endosomal compartments in greater detail. We noticed that MVEs were not uniformly distributed within tapetal cells. By measuring the shortest distance between individual MVEs and the plasma membrane in electron micrographs of WT tapetal cells at the free microspore stage, we found that over 85% of the MVEs were located within 2 microns from the plasma membrane domains facing the locule, which are devoid of a cell wall (Figure 5, A–C). A similar distribution pattern was seen in *ist11 lip5* double mutant tapetal cells, with over 80% of the MVEs found in the vicinity of the locule-facing plasma membrane regions (Figure 5, A–C). To determine whether other organelles show similar asymmetric distribution patterns within tapetal cells, we also analyzed the relative positions of mitochondria with respect to the plasma membrane facing the locule (Supplemental Figure S5). We found that mitochondria were more evenly distributed than MVEs, with approximately 48% of mitochondria within 2 microns from the plasma membrane in both WT and double mutant tapetal cells.

We then analyzed the structural features of MVEs. In WT plants, MVEs in tapetal cells (380 ± 48 nm in diameter) were significantly larger than those found in root cells (285

nm \pm 45 nm in diameter (Buono et al., 2016) and in microspores (220 ± 48 nm in diameter; Figure 5, D–G). Interestingly, whereas the *ist11 lip5* double mutation did not affect the size of MVEs in root cells, MVEs were significantly smaller (224 ± 53 nm) in mutant tapetal cells but significantly larger (290 ± 72 nm) in microspores compared to the corresponding WT cell types (Figure 5F). In addition, endosomal intraluminal vesicles of root cells (Buono et al., 2016), tapetal cells, and microspores were significantly enlarged in the *ist11 lip5* mutant, whereas intraluminal vesicles in WT tapetal endosomes were 48 ± 7 nm, they were 55 ± 8 nm in the *ist11 lip5* double mutant (Figure 5G). Likewise, the diameter of endosomal intraluminal vesicles in microspores was 55 ± 13 nm in WT but significantly larger (69 ± 16 nm) in the *ist11 lip5* mutant (Figure 5G). Finally, we found that tapetal MVEs contained fewer intraluminal vesicles per cross section than the WT (Figure 5H). These results indicate that the *ist11 lip5* double mutation affects intraluminal vesicle size consistently across cell types, whereas changes in endosomal size are cell type-dependent. We do not believe that the differences in MVE structure between tapetal and root cells were due to different temperature conditions (previous root MVE analysis was performed in seedlings grown at 22°C, whereas tapetal MVEs were from anthers grown at 28°C) because MVE structural features were similar in WT tapetal cells and pollen grains from anthers grown at either 22°C or 28°C.

In MVEs of root cells, intraluminal vesicles form in concatenated networks that are critical for cargo retention and proper endosomal sorting; single mutants for late ESCRT1 components such as CHMP1 and LIP5 show reduced vesicle concatenation (Buono et al., 2017). To further understand the defects in MVE function in mutant tapetal cells, we performed electron tomography and 3D segmentation. Based on the reconstruction of 8 WT and 12 *ist11 lip5* mutant MVEs, we found that whereas approximately 90% of the endosomal intraluminal vesicles in WT tapetal cells were concatenated as part of complex network, the large majority (9 out of 12) of the reconstructed *ist11 lip5* endosomes contained only nonconcatenated vesicles of either free vesicles or single buds attached to the limiting membrane (Figure 6, A–C), which is a much more acute reduction in vesicle concatenation than previously reported for MVEs in root cells of *chmp1* or *lip5* single mutants (Buono et al., 2017). In addition, and consistent with our transmission microscopy analysis (Figure 5), the reconstructed *ist11 lip5* mutant MVEs showed a sharp decrease in the number of intraluminal vesicles compared to their WT counterparts (Figure 6, A and B).

Interestingly, we also observed that, besides the structural defects in MVEs where ESCRT function is needed for cargo sorting and vesicle formation, the early endosomes/TGN compartments were structurally abnormal in *ist11 lip5* mutant tapetal cells. Whereas TGN profiles associated with Golgi stacks and clusters of MVEs were detected in both WT and mutant cells, the TGN in *ist11 lip5* tapetal cells showed large marginal bulges of up to 250 nm in diameter

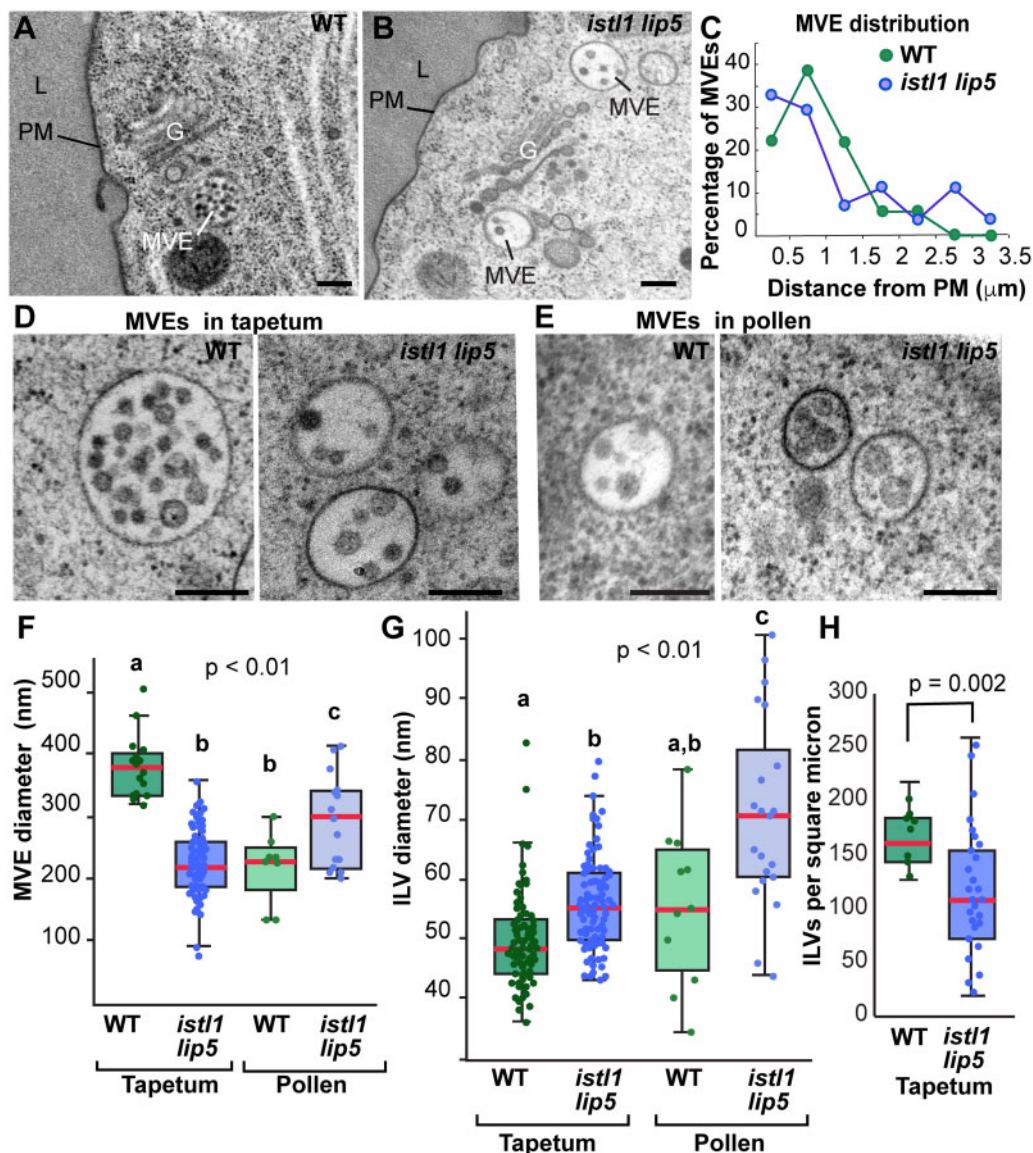


Figure 5 MVE distribution and morphology in the tapetum and pollen. A, B, Representative images of MVEs in tapetal cells near the locule-facing plasma membrane (PM) regions of WT (A) and *istl1 lip5* (B). Microspores have been just released from tetrads at this stage. C, Analysis of MVE distribution in the tapetum. The graph depicts the frequency of MVEs at increasing distances from the PM. All MVEs found in single sections of five tapetal cells during microspore development were analyzed (17 WT MVEs and 27 *istl1 lip5* mutant MVEs). D, E, The overview of MVEs in tapetal cells during microspore development (D) and developing (early bicellular) pollen (E) in WT and *istl1 lip5* anthers. F–H, Quantitative analysis of MVE structural features in the tapetum and developing pollen, showing differences in MVE diameter (F), intraluminal vesicle (ILV) diameter (G), and number of ILVs per square micron in tapetal MVEs (H). The boxes show the 25th and 75th percentiles, middle lines indicate the median, and whiskers refer to upper and lower fences. Different letters represent significant differences by one-way ANOVA followed by Tukey (Supplemental File 1) in (F) and (G). Statistical significance in (H) was calculated by a two-tailed Student's *t* test. G, Golgi; L, locule. Scale bars = 200 nm.

(Figure 7), suggesting a role of ISTL1 and LIP5 in TGN function.

Localization of GFP-ABCG9 and GFP-ABCG16 in *istl1 lip5* tapetal cells

As both exine and tryphine deposition depend on the secretory activity of tapetal cells, we tested whether the localization of the transporters ABCG9 and ABCG16, both of which localize to the plasma membrane of tapetal cells and

participate in pollen wall assembly (Choi et al., 2014; Yim et al., 2016), were affected in the double mutant. We confirmed that both transporters localized to the plasma membrane in WT tapetal cells. However, whereas GFP-ABCG16 was found at the plasma membrane of *istl1 lip5* tapetum, GFP-ABCG9 was largely absent from it (Figure 8).

We then looked more carefully at the localization of GFP-ABCG9 and GFP-ABCG16 in mutant anthers. Whereas the single *istl1* mutant tapetal cells showed normal distribution

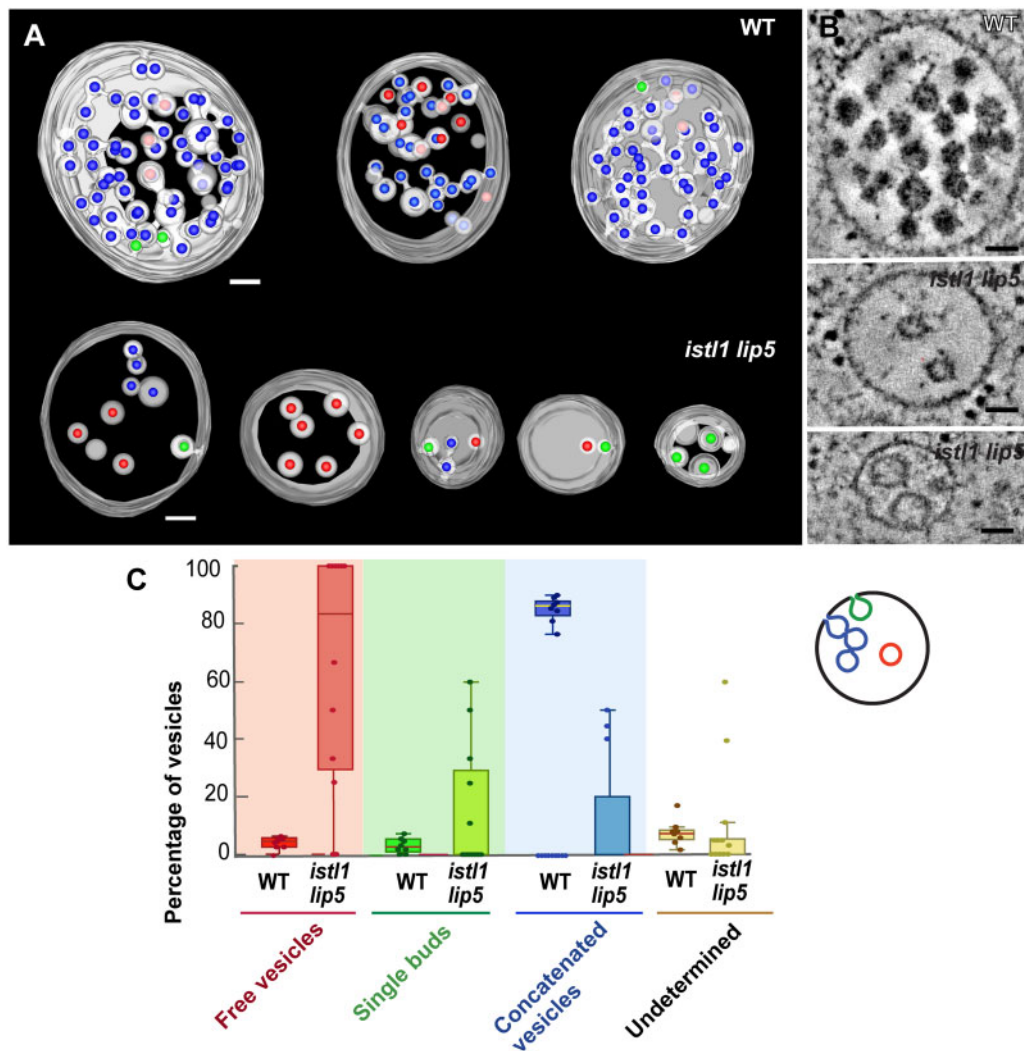


Figure 6 Tomographic analysis of MVEs and TGNs in *ist1 lip5* tapetal cells during the free microspore stage. A, Tomographic reconstructions of WT and *ist1 lip5* MVEs. Colored spheres were placed within ILVs to better visualize concatenated vesicles (blue), single buds attached to the limiting membrane (green), and free vesicles (red). B, Representative tomographic slices of MVEs. C, Quantification of vesicle connections derived from 8 WT and 12 *ist1 lip5* reconstructed MVEs. The boxes show the 25th and 75th percentiles, middle lines indicate the median, and whiskers refer to upper and lower fences. Scale bars = 50 nm.

of GFP-ABCG9, both *lip5* and *ist1 lip5* exhibited an increase in internal signal, more specifically in the tonoplast (Figure 8A), which is typical of endosomal sorting mutants (Spitzer et al., 2009; Buono et al., 2016). However, different from the single *lip5* mutant, *ist1 lip5* tapetal cells were largely devoid of GFP-ABCG9 signal at the plasma membrane but showed more signal associated with internal membranes besides the tonoplast (Figure 8, A and B). This suggests that, whereas both *lip5* and *ist1 lip5* tapetal cells show defects in endosomal sorting, the *ist1 lip5* mutant is unable to achieve and/or maintain the plasma membrane localization of GFP-ABCG9. Although some GFP-ABCG16 signal was also detected in the tonoplast of double mutant tapetal cells, its overall localization at the plasma membrane was normal and indistinguishable from the WT (Figure 8, C and D).

This drastic discrepancy between the effects of the double *ist1 lip5* mutation on the trafficking of two ABCG

transporters in tapetal cells prompted us to check more carefully the temporal expression of these two proteins. We found that whereas GFP-ABCG16 was expressed during the late microspore mother cell and tetrad stages (stages 6 and 7 of Arabidopsis anther development; Sanders et al., 1999) and degraded in the tapetal vacuoles when microspore are released into the locule (stages 8 and 9; Figure 8C), GFP-ABCG9 was expressed at stages 9 and 10. This suggests that the role of ISTL1 and LIP5 in the proper localization of plasma membrane proteins in tapetal cells may be critical only when microspores are free in the locule but not in earlier developmental stages.

To test whether exocytosis of soluble proteins was affected in *ist1 lip5* mutants, we expressed a GFP-tagged type III LTP (At5g62080) that is specifically expressed in tapetal cells and secreted to the anther locule during pollen formation (Huang et al., 2013). In both the WT and *ist1 lip5*

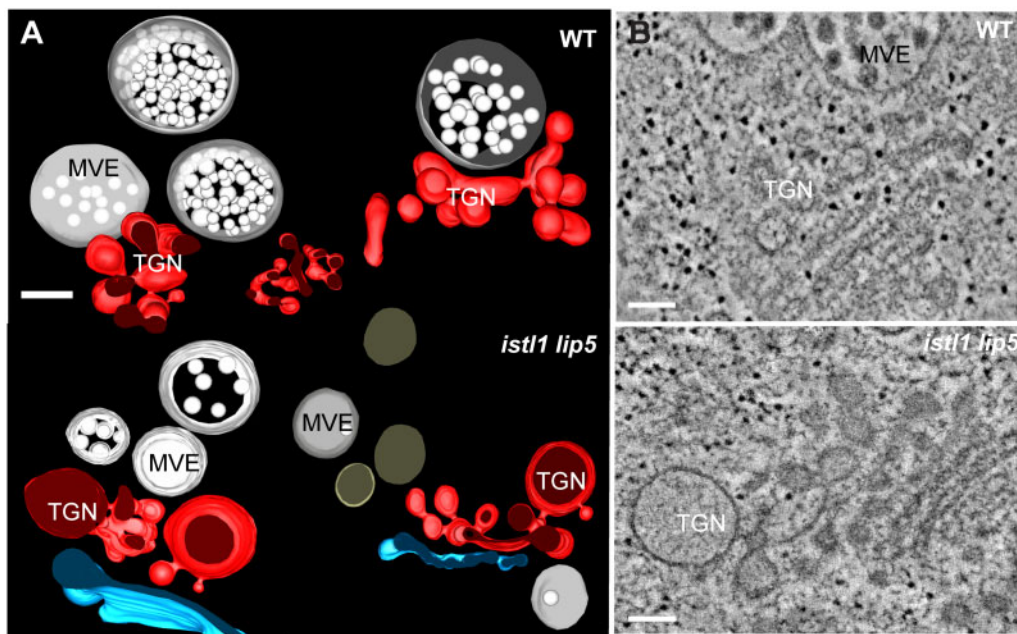


Figure 7 Tomographic analysis of TGNs in WT and *ist1 lip5* mutant tapetal cells at the free microspore stage. A, Tomographic reconstructions and B, tomographic slices of WT and *ist1 lip5* TGNs (red) and associated MVEs (white). For simplicity, ILVs are depicted as spheres within MVEs. Note large marginal bulges in the mutant TGNs. The trans-most Golgi cisterna is depicted in cyan. Scale bars = 100 nm.

anthers, LTP-GFP first accumulated in tapetal cells and was first detected in the locule at the tetrad stage (stage 7; Figure 9A). Secretion continued through the free microspore stages until the onset of tapetal degeneration (stages 8–10). However, by stage 9, LTP-GFP accumulated inside the tapetal vacuoles in the double mutant but not in WT, suggesting that exocytosis of LTP-GFP was impaired in mutant tapetal cells at this stage (Figure 9A). These results, together with the analysis of the two ABCG transporters (Figure 8), further support the notion that exocytosis of both plasma membrane and secreted cargo is compromised in *ist1 lip5* tapetal cells, specifically during the free microspore stage.

To further confirm the specific defects on exocytosis seen in *ist1 lip5* tapetum, we analyzed the distribution of the soluble bulk-flow secretion marker sec-RFP, which contains a sporamin signal peptide and is exported to the apoplast in plant cells (Samalova et al., 2006). Defects in exocytosis result in retention of sec-RFP in the endomembrane system (Renna et al., 2013). In root cells, sec-RFP was exported to the apoplast both in WT and *ist1 lip5* seedlings (Figure 9, B and C). However, the sec-RFP signal in *ist1 lip5* anthers accumulated in intracellular foci of tapetal cells at the free microspore stage (Figure 9, D–G). These results confirm the notion that in the tapetum, ISTL1 and LIP5 are required for exocytosis, a surprising function for ESCRT components.

ESCRT gene expression in tapetum, microspores, pollen, and root cells

We have found that ISTL1 and LIP5 together play a key role in exocytosis in a cell type- and developmentally dependent manner. To explore whether this unusual function is

connected to the expression of specific sets of ESCRT genes, we compared transcriptomic data from root cells (developing cortex and meristematic cells; Li et al., 2016), microspores (Wang et al., 2020), pollen grains (Loraine et al., 2013), and tapetal cells at two stages of development (stages 6 and 7 and stages 8–10; Li et al., 2017; Supplemental Figure S6).

Although none of the 52 ESCRT genes considered in this analysis was specifically expressed or not expressed in tapetal cells, based on the overall expression analysis, tapetal cells were clustered together in a different clade from roots, microspores, and pollen grains (Supplemental Figure S6), suggesting that differences in the expression patterns of multiple ESCRT genes could be the underlying reason for their unique function in tapetal cells. Both *ISTL1* and *LIP5* were expressed at similar levels in all six cell types/stages, with the exception of pollen grains, where *LIP5* expression was lower. Interestingly, *LIP5* and *ISTL1* were expressed in the two tapetum stages analyzed, and their expression slightly increased at the latest stage, when exocytosis was impaired in the double mutant.

Discussion

We have identified a role for two ESCRT components, ISTL1 and LIP5, in regulating exocytosis during the late stages of tapetal function. Double *ist1 lip5* mutant microspores and pollen grains can develop normally only if at least one WT allele of either gene is expressed in the tapetal cells. The combined functions of these two genes extend beyond their known canonical functions in MVE sorting, as they are required for exocytosis of both plasma membrane and

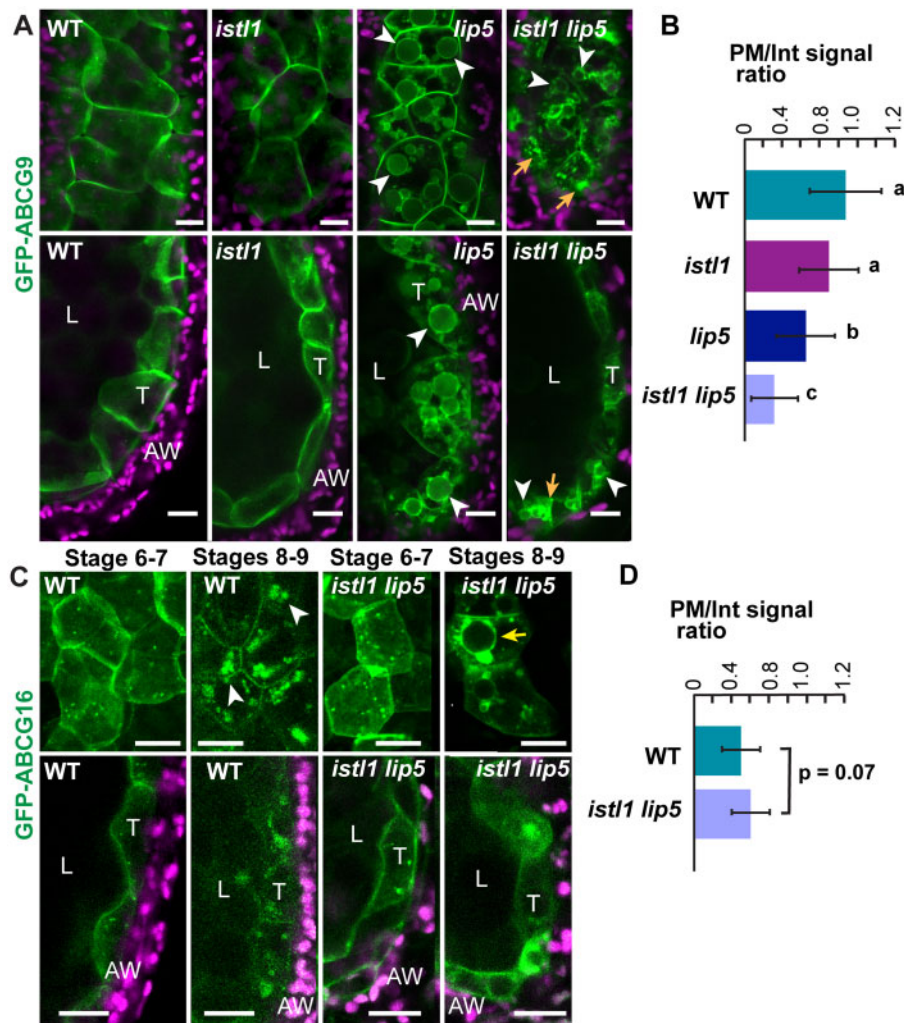


Figure 8 Localization of GFP-ABCG9 and GFP-ABC16 in tapetal cells. A, Confocal slices of tapetal cells collected from the surface of the tapetal layer (tangential view; upper row) and through the middle of the locule (bottom row) in WT (WT), *istl1*, *lip5*, and *istl1 lip5* mutant anthers at the free microspore stage (stages 8 and 9). Chlorophyll autofluorescence is shown in magenta. Note the accumulation of GFP-ABCG9 at the tonoplast of small vacuoles in the *lip5* and *istl1 lip5* cells (white arrowheads) and in internal foci in the *istl1 lip5* tapetum (orange arrows). B, Quantification of the ratio between the GFP-ABCG9 signal intensity from the PM and cell interior (Int) shown as mean \pm SD. A smaller ratio indicates more intracellular signal. Different letters represent significant differences (one-way ANOVA followed by Tukey, $P < 0.05$; $n = 40$ cells from 7 WT anthers, 18 cells from 5 *istl1* anthers; 30 cells from 6 *lip5* anthers; 59 cells from 8 *istl1 lip5* anthers; see Supplemental File 1). C, Confocal slices from the surface of the tapetal layer (tangential view; upper row) and through the middle of the locule (bottom row) in WT and *istl1 lip5* mutant anthers at different stages of development. By stages 8 and 9, GFP-ABC16 is removed from the PM and delivered to either the vacuolar lumen for degradation in WT tapetal cells (white arrowheads) or partially mis-sorted to the tonoplast in *istl1 lip5* tapetal cells (yellow arrow). D, Quantification of the ratio between the GFP-ABC16 signal intensity from the PM and Int shown as mean \pm SD at stages 6 and 7 ($n = 29$ cells from four WT anthers; 45 cells from 12 *istl1 lip5* anthers). A *t* test was used to calculate the corresponding *p* value. AW, anther wall; T, tapetum. Scale bars = 10 μ m.

secreted proteins at the stage when microspores are free in the anther locule.

Impaired exocytosis in tapetal cells of *istl1 lip5* anthers

In both single and double *istl1 lip5* mutants, tapetum development and programmed cell death proceed normally. Programmed cell death and the loss of plasma membrane integrity cause the release of the tapetal cell contents into the locule for their incorporation into the pollen grain exine as part of the tryphine (Pacini et al., 1985). However, the

export of tryphine components from tapetal cells into the locule starts earlier through the activity of plasma membrane-localized transporters, many of which are exclusively expressed in tapetal cells (Choi et al., 2014).

We found that one of those transporters, ABCG9, is largely absent from the plasma membrane of *istl1 lip5* tapetal cells but instead accumulates in internal membranes, including the tonoplast. Whereas mis-sorting of plasma membrane proteins to the tonoplast is a common defect in ESCRT mutants, including the *lip5* single mutant (Spitzer et al., 2009; Buono et al., 2016), the inability to maintain their

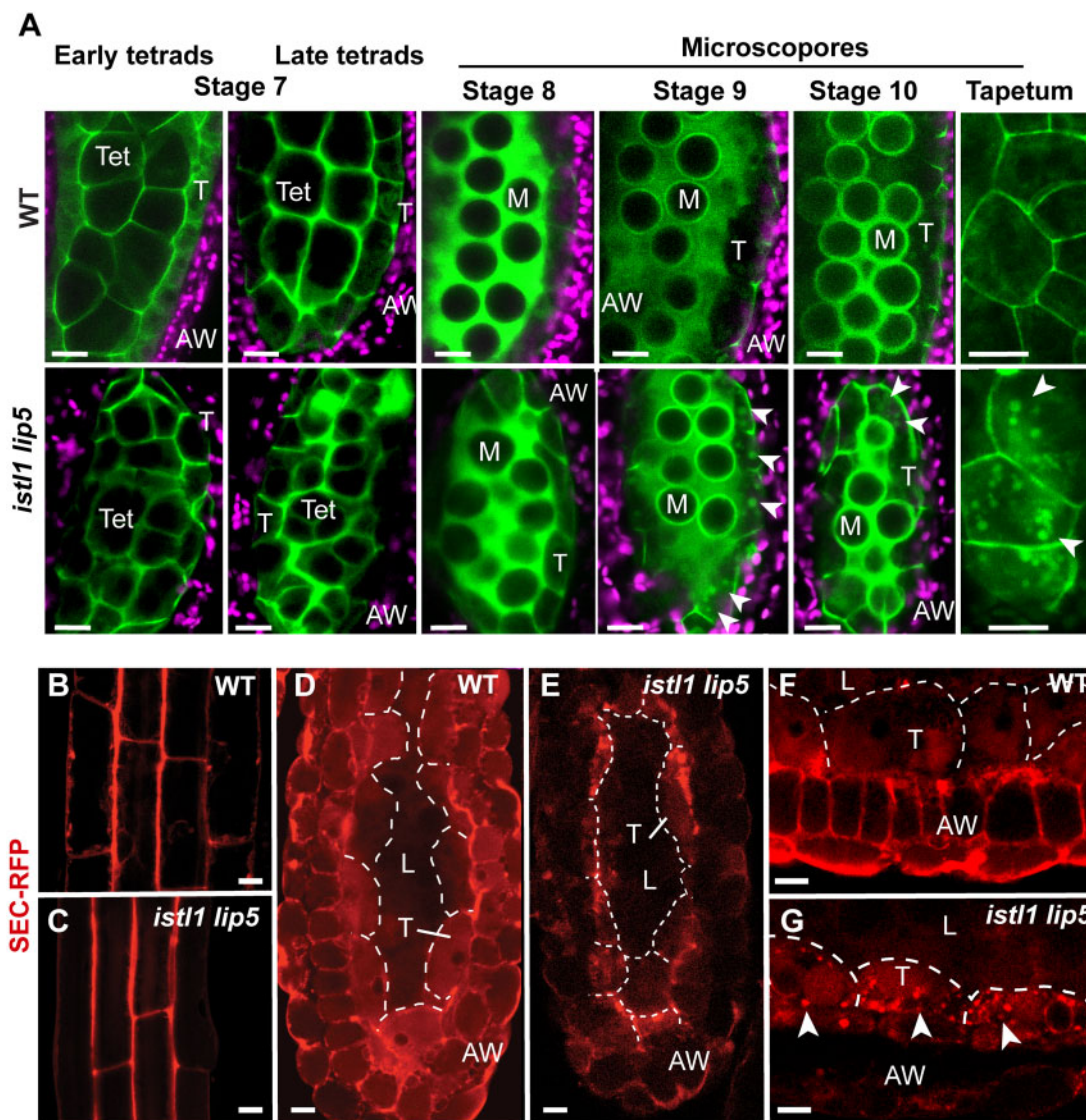


Figure 9. Secretion of soluble cargo by tapetal cells. **A**, Expression and secretion of LTP-GFP in WT and *istl1 lip5* mutant anthers. LTP-GFP secretion into the locule is first detected in the early tetrad stage and until tapetum degeneration at late stage 10. LTP-GFP accumulates inside tapetal vacuoles (white arrowheads) at stages 9 and 10 in *istl1 lip5* mutant but not the WT anthers. **(A)–(G)** Distribution of the sec-RFP secretory reporter. **B**, **C**, Apoplast localization of sec-RFP in both WT and *istl1 lip5* mutant roots cells. **D–G**, Distribution of sec-RFP in WT and *istl1 lip5* mutant anthers (**D**,**E**) and tapetal cells (**F**,**G**) at the free microspore stage (stage 9). Note the abnormal accumulation of sec-RFP in mutant tapetal cells (arrowheads in **F**). M, microspore; Tet, tetrad. Scale bars = 10 μ m.

plasma membrane localization is not. The finding that *lip5* mutant tapetal cells are able to support normal microspore/pollen grain development indicates that the mis-sorting of GFP-ABCG9 to the tonoplast does not result in inadequate tapetal secretory activity. However, the drastic reduction in the plasma membrane pool of GFP-ABCG9 is only seen in the *istl1 lip5* mutant could account for the abnormalities in pollen development. ABCG9 works redundantly with ABCG31 to export tryphine components (steryl glycosides) from the tapetum into the locule, and a double mutant plant for both transporters showed an approximately 35% reduction in pollen viability, with largely normal exine patterns but irregular tryphine containing crystalline electron-lucent structures (Choi et al., 2014), similar to the ones

observed in *istl1 lip5* anther locules. Mutants for some other tapetum-specific, plasma membrane-localized ABCG transporters show even more severe pollen defects. For example, mutants for the ABCG26 transporter, which exports sporopollenin precursors from tapetal cells into the locule, produce aborted microspores with no exine (Quilichini et al., 2010), whereas mutants for ABCG16 and ABCG1 produce aborted pollen grains with no nexine layer within the exine and a grossly abnormal intine (Yadav et al., 2014; Yim et al., 2016). The finding that over 80%–90% of the microspores in the *istl1 lip5* double mutant develop an exine with normal or slightly altered patterns (Figure 2, A and B) indicates that sporopollenin deposition and therefore, the trafficking of at least some ABCG transporters is not

drastically affected in the double mutant. Consistent with this notion, we found that the ABCG16 transporter is normally localized to the plasma membrane of tapetal cells in double mutant anthers. However, the temporal expression patterns of these ABCG transporters differ according to the biosynthetic functions of the tapetum. ABCG16, which is important for exine and intine assembly, is expressed during early stages, when microspores are still enclosed in tetrads surrounded by callose (stages 6 and 7; Figure 8C), whereas ABCG9 is expressed later, when the microspores are free in the locule (stages 8 and 9; Figure 8A). These observations suggest that LIP5 and ISTL1 specifically control the plasma membrane localization of proteins in the tapetum at later development stages (stages 9 and 10), when tryphine components start to be released into the locule. In support of a general block of exocytosis in late tapetal cells, we found that a type III LTP was secreted normally into the locules of *istl1 lip5* anthers until the free microspore stage, when LTP-GFP was redirected to the vacuolar lumen (Figure 9A).

Unfortunately, we were unable to analyze tryphine composition in the double *istl1 lip5* mutant to determine which additional transporter activities could be compromised in the tapetum. The analysis of waxes from whole anthers showed differences for some minor components (alkanes and sterols) between the WT and mutants and between single and double mutants, but compared to the small amount of tryphine contained in each anther, it is most likely that our analysis failed to capture relevant differences in the secretion of tryphine wax components.

How ISTL1 and LIP5 control exocytosis of plasma membrane and secreted proteins at the free microspore stage is unclear. However, it is important to note that this is not an expected result for a stronger, synergistic effect of the two mutations on ESCRT function through MVE sorting. The strong ESCRT mutant *chmp1a chmp1b* partially mis-sorts all types of plasma membrane proteins to the tonoplast, resulting in embryo or seedling lethality (Spitzer et al., 2009). However, although the lack of CHMP1 function leads to more severe developmental defects than the double *istl1 lip5* mutation, it does not result in plasma membrane depletion of any of the several ESCRT cargo proteins that have been analyzed (Spitzer et al., 2009). In addition, although LIP5 and ISTL1 are not differentially or even preferentially expressed in the tapetum (Supplemental Figure S6), their combined function is specifically important to tapetal cells, whereas the functions of other cell types and tissues seem to be much less affected by the double mutation. This points to a function of the ISTL1 and LIP5 proteins in tapetal cells.

Our data suggest that ISTL1 and LIP5 together have a role in the endomembrane anterograde pathway that is more critical in the tapetum than in other cell types. There is an additional evidence in the literature that the secretory activity of tapetal cells is regulated in specific manners. For example, COP-II vesicle assembly is required for anterograde trafficking from the ER to the Golgi. There are two isoforms of the COPII component SEC31 in Arabidopsis, SEC31A and

B, which are widely expressed in plant organs during development. However, a mutant for SEC31B shows normal growth and development but severe defects in exine assembly and tryphine deposition, with tapetal cells that fail to form tapetosomes while maintaining a normal ABCG9 pool (Zhao et al., 2016). Thus, the high secretory activity of tapetal cells may be associated with specialized and unique functions of trafficking factors, including ESCRT proteins.

ISTL1 was recently identified as a candidate important for maize (*Zea mays*) leaf cuticle development in a genome-wide association study (Lin et al., 2020). Cuticle assembly on the surface of all aerial organs requires the export of cutin precursors waxes from epidermal cells and relies on ABCG transporters closely related to those involved in the export of exine and tryphine components (McFarlane et al., 2010; Panikashvili et al., 2010, 2011). Our wax analysis of whole anthers showed that even though single *istl1* and *lip5* mutants have fully functional anthers, they do have reduced accumulation of some wax alkanes and sterols, opening the possibility that LIP5 and ISTL1 may play a role in the exocytosis of plasma membrane transporters associated with the export of cuticle and waxes in other cell types.

We also detected ovule and seed abortion due to maternal effects in *istl1 lip5* plants. Although we did not investigate these developmental defects in detail and there are no equivalent cells to tapetal cells within ovules, megaspore mother cells become surrounded by callose prior to undergoing meiosis, and female gametophyte/embryo sac development requires the intense transport of nutrients and signaling molecules from maternal tissues (Webb and Gunning, 1990). ISTL1 and LIP5 could be required to mediate these activities.

Endosomes in tapetal cells and microspores

We also found some interesting features in the distribution and structure of MVEs of tapetal cells. The distribution of MVEs was not uniform across the cytoplasm but rather polarized toward the plasma membrane regions facing the locule, which could be important for trafficking endocytic material and mediating the efficient turnover of plasma membrane proteins.

Tapetal MVEs were larger and more complex in terms of number of intraluminal vesicles than those in either root cells (Buono et al., 2017) or microspores/pollen. Some studies suggest that changes in endocytosis correlate with MVE size and number. For example, in shoot apical meristem cells, MVE size and abundance increase during cytokinesis (Segui-Simarro and Staehelin, 2006), when up to 75% of the cell plate membrane is removed by endocytosis (Otegui and Staehelin, 2000). Similarly, MVEs increase in size in concert with two waves of endocytic activity that occur during ovulation in *C. elegans* (Frankel et al., 2017). Thus, the larger size of MVEs in tapetal cells compared to root cells could be related to the high turnover of plasma membrane proteins likely required to sustain the secretory activity of the tapetum. Another possibility is that MVE size correlates to the cell ploidy. In fact, tapetal cells with two polyploid nuclei

develop the largest MVEs, haploid microspores contain the smallest MVEs, and the diploid differentiating root cortex cells contain MVEs of intermediate size. Whereas the mechanisms that regulate MVE size are not known, it is noteworthy that the double *ist1 lip5* mutation affects MVE diameter in a cell-specific manner. Thus, whereas MVE diameter was not altered in *ist1 lip5* root cell, MVEs were smaller in mutant tapetal cells but larger in mutant pollen grains compared to the corresponding WT cell types.

Different from MVE diameter, the intraluminal vesicles were larger in all the analyzed cell types of the *ist1 lip5* double mutant vs. the WT. In addition, we found a drastic reduction in vesicle concatenation in *ist1 lip5* tapetum. Most *ist1 lip5* MVEs contained only free vesicles or single buds attached to the limiting membrane (Figure 6), which represents the lowest vesicle concatenation rate detected in any cell type or ESCRT mutant, including *lip5* (Buono et al., 2017).

We also noticed structural alterations in early endosomes/TGNs of *ist1 lip5* tapetal cells. This finding is unexpected, as no other plant ESCRT mutation has been reported to affect TGN morphology. However, mutants for TGN-localized proteins that are important for secretion/exocytosis often show structural alterations in the TGN. For example, mutants for ECHIDNA, which controls cuticular wax secretion in Arabidopsis epidermal cells (McFarlane et al., 2014), pollen and anther development (Fan et al., 2014), and general secretory trafficking (Gendre et al., 2011) show abnormal TGN morphology (Boutte et al., 2013). In addition, loss-of-function mutants for TGNap1, which maintains homeostasis of biosynthetic and endocytic trafficking pathways and is also required for the proper secretion of sec-RFP (Renna et al., 2018), showed bulges in the TGN similar to those observed in *ist1 lip5* tapetal cells. Taken together, the structural alteration of the TGN further supports a role for ISTL1 and LIP5 in exocytosis.

Materials and methods

Plant materials and growth conditions

The following *A. thaliana* lines were used in this study: *lip5-1* (SAIL_854_F08; Haas et al., 2007), *ist1-1* (SALK_021562; Buono et al., 2016), and *sid2-2* (Wildermuth et al., 2001). Expression cassettes containing *ACBG9pro::sGFP-ABCG9* (Choi et al., 2014), *ABCG16pro::GFP-ABCG16* (Yim et al., 2016), or *GFP-LTP (pAt5g62080::At5g62080-GFP)* (Huang et al., 2013) were introduced into Col-0 and *ist1 -/- lip5 +/-* by *Agrobacterium*-mediated transformation and crossed with *lip5* to obtain homozygous *lip5* mutant plants. The fluorescent protein markers VHAa1-GFP (Dettmer et al., 2006), RabF2a-GFP (WAVE7; (Geldner et al., 2009)), and sec-RFP (Samalova et al., 2006) were introduced into the mutant lines by crossing.

Plants were grown in growth chambers at 22°C or 28°C under 16 h of light (fluorescent lights; 120 $\mu\text{m m}^{-2} \text{s}^{-1}$) and 8 h of dark cycle. Seeds were pretreated with 70% ethanol for 10 min, surface-sterilized in 25% concentrated bleach

for 1 min, and washed in distilled water at least four times. Seeds were sown on plates containing 0.5 \times Murashige and Skoog salts supplemented with 1% sucrose, stratified at 4°C for 2–4 days, and set to germinate.

Pollen viability assay

Alexander's staining of pollen was performed as previously described (Peterson et al., 2010). Briefly, flower buds were fixed in Carnoy's fixative (6 ethanol:3 chloroform:1 acetic acid) with brief vacuum infiltration for 2 h. Following fixation, anthers were quickly dissected from the bud on a microscope slide in a drop of fixative, and a few drops of Alexander's staining solution (10 mL 95% ethanol, 1 mL of 1% solution malachite green in 95% ethanol, 25-mL glycerol, 5 mL of 1% acid fuchsin in water, 0.5 mL of 1% solution Orange G in water, 4-mL glacial acetic acid, and distilled water to a total of 100 mL) were added to the sample. A coverslip was placed on top and the slide was placed on a hot plate for a few seconds. Images were captured on an Olympus BX60 epifluorescence microscope and analyzed using Fiji (Schindelin et al., 2012).

Transmission electron microscopy and electron tomography

Anthers were high-pressure frozen/freeze-substituted for transmission electron microscopy. Anthers at various stages of development were dissected and frozen in a Baltec HPM 010 high-pressure freezing machine. For ultrastructural analysis, samples were quick-freeze substituted in 2% (w/v) OsO₄ in anhydrous acetone at –80°C overnight, followed by warming to room temperature on a rocker with slow agitation for 3–4 h and incubation at room temperature for ~1 h. After several acetone rinses, the samples were infiltrated in a series of Epon resin (Electron Microscopy Sciences) changes (10% [v/v] resin in acetone, 25%, 50%, 75% over the course of several hours and three 100% exchanges of 12 h, 3 h, 3 h) before embedding and polymerizing at 60°C for 24 h. Morphological measurements were done using Fiji (Schindelin et al., 2012).

For electron tomography, 300-nm-thick sections of EPON-embedded high-pressure frozen/freeze-substituted anthers were mounted on formvar-coated copper slot grids and stained with 2% uranyl acetate in 70% methanol and Reynold's lead citrate (2.6% lead nitrate and 3.5% sodium citrate, pH 12). Colloidal gold particles 15 nm in diameter were used as fiducial markers to align the series of tilted images. The sections were imaged in a Tecnai TF30 intermediate voltage electron microscope (Thermo Fisher) operated at 300 kV. The images were taken from +60° to –60° at 1.0° intervals along two orthogonal axes (Mastronarde, 1997) and collected with a US1000 camera (Gatan) at a pixel size of 0.558 nm. Tomograms were computed using the simultaneous iterative reconstruction technique (Gilbert, 1972) using the IMOD software package (Kremer et al., 1996). Tomograms were displayed and analyzed with 3Dmod, the graphic component of the IMOD software

package. The thinning factor for each tomogram was calculated and corrected in the models.

Scanning electron microscopy

Scanning electron microscopy was performed on a FEI Quanta 200 under high vacuum. Mature pollen from open anthers was adhered to stubs without fixation and coated with a 5 nm layer of platinum using a Leica EM ACE600 High Vacuum Sputter Coater.

Confocal laser scanning microscopy

Fluorescent confocal images were captured using a Zeiss model no. LSM 780 or LSM 710 with a $\times 20$ objective (Plan-Apochromat NA = 0.8, Carl Zeiss) or $\times 40$ objective (LD C-Apochromat NA = 1.1 or C-Apochromat NA = 1.2, water-immersion, Carl Zeiss). GFP was excited using a 488 nm argon laser and emission collected from 490 to 597 nm using a 488/561/633 MBS filter (Carl Zeiss). Chlorophyll was excited by a 633 helium–neon laser and emission collected from 647 to 721 nm. Sec-RFP was excited using a 514 nm argon laser and emission collection at 531–703 nm using a 458/514 MBS filter (Carl Zeiss). Anthers were dissected according to bud size and corresponding to stage as described previously (Sanders et al., 1999). Quantification of confocal images was done with FIJI (Schindelin et al., 2012)

Anther wax extraction and analysis

Approximately 50 anthers per replicate of the Col-0 control and each of the mutant plants were harvested, immediately frozen, and lyophilized until further use. Each replicate was placed in glass tubes, immersed in 5-mL chloroform, and extracted for 1 min by gently inverting the tube. After transferring the extract to a new tube, 1 μ g of each internal standard, namely n-tetracosane (24:0 alkane), 1-pentadecanol (15:0-OH), and heptadecanoic acid (17:0) were added to each sample. The chloroform extracts were evaporated under a nitrogen stream.

Wax extracts were chemically treated to form trimethylsilyl ester and ether derivatives as described previously (Razeq et al., 2014). After resuspending each derivatized sample in 200- μ L hexane, the samples were transferred to GC vials with inserts and analyzed by GC–MS on a TRACE 1300 Thermo Scientific GC with a Thermo Scientific ISQ Single Quadrupole MS detector. Splitless injection was used with a TG-5MS capillary column (30 m \times 0.25 mm i.d., and 0.10 μ m film thickness) and a helium flow set at 1.0 mL min^{-1} . Temperature settings were as follows: inlet 330°C, detector 300°C, oven temperature set at 150°C for 3 min and then increased to 300°C at a rate of 4°C min^{-1} , with a final hold at 300°C for 5 min. Wax components were identified by their relative retention times and characteristic mass spectra.

ESCRT gene expression analysis

Gene expression analysis of Arabidopsis ESCRT genes was performed using publicly available RNA-sequencing data from pollen (Loraine et al., 2013; NCBI database Sequence

Read Archive accession number SRP022162), microspores (Wang et al., 2020; Gene Expression Omnibus (GEO) accession number GSE129744), tapetum (Li et al., 2017; GEO accession number GSE102528), and root tissues (developing cortex and meristem; Li et al., 2016; BioProject accession number PRJNA323955). To make the RNA-sequencing data comparable across different tissues, the relative expression unit (FPKM or Fragments Per Kilobase of transcript per Million mapped reads) was converted to TPM (Transcripts Per Million). Then, $\log(\text{TPM} + 1)$ was calculated and plotted using the heatmap.2 function (<https://cran.r-project.org/web/packages/gplots/index.html>) in R (<https://www.r-project.org>).

Statistical analysis

Statistical analysis was performed in Microsoft Excel unless otherwise stated. Unpaired two-tailed Student's *t* test was used to compare means from two groups, and one-way analysis of variance (ANOVA) used for multiple comparisons with a post hoc Tukey test conducted using an online calculator (astatsa.com) and with GraphPad Prism (<https://www.graphpad.com/scientific-software/prism/>). Statistical data from relevant figures are provided in Supplemental File S1.

Accession numbers

Sequence data from this article can be found in the GenBank/EMBL libraries under the following accession numbers: *LIP5* (AT4G26750); *ISTL1* (AT1G34220); *SID2* (AT1G74710); *ABCG9* (AT4G27420); *ABCG16* (AT3G55090); and *LTP* (AT5G62080).

Supplemental data

The following materials are available in the online version of this article.

Supplemental Figure S1. Pollen viability in *istl1 lip5 sid2* anthers from plants grown at 22°C.

Supplemental Figure S2. Transmission electron micrographs of abnormally vacuolated and collapsed pollen grains in *istl1 lip5* anthers.

Supplemental Figure S3. Anther wall development.

Supplemental Figure S4. Confocal imaging of MVE and TGN markers in the tapetum.

Supplemental Figure S5. Distribution of mitochondria in tapetal cells.

Supplemental Figure S6. ESCRT gene expression in different cell types.

Supplemental File S1. ANOVA tables.

Acknowledgments

We would like to thank Dr Youngsook Lee (Pohang University of Science and Technology, Korea) for providing the *ACBG9pro::GFP-ABCG9* and *ACBG16pro::GFP-ABCG16* expression vectors, Drs Ming-Der Huang (National Sun Yat-sen University, Taiwan) and Anthony Huang (University of California Riverside) for the *pAt5g62080::At5g62080-GFP* vector, and Dr Federica Brandizzi (Michigan State University) for

providing seeds of the sec-RFP line. We are also grateful to Dr Makoto Yanagisawa (UW-Madison) for his assistance transforming *Arabidopsis* plants.

Funding

This work was funded by NSF (grant no. MCB1614965 to M.S.O.); funds from the Botany Department (UW-Madison) to K.G. and from the Morgridge Institute for Research to P.G.A.; and in part, by funding from the Canada Research Chairs program and the Natural Sciences and Engineering Research Council (NSERC) of Canada to I.M.

Conflict of interest statement. None declared.

References

- Alexander MP** (1969) Differential staining of aborted and non-aborted pollen. *Stain Technol* **44**: 117–122
- Ariizumi T, Toriyama K** (2011) Genetic regulation of sporopollenin synthesis and pollen exine development. *Annu Rev Plant Biol* **62**: 437–460
- Azmi IF, Davies BA, Xiao J, Babst M, Xu Z, Katzmann DJ** (2008) ESCRT-III family members stimulate Vps4 ATPase activity directly or via Vta1. *Dev Cell* **14**: 50–61
- Belda-Palazon B, Rodriguez L, Fernandez MA, Castillo MC, Anderson EA, Gao C, Gonzalez-Guzman M, Peirats-Llobet M, Zhao Q, De Winne N, et al.** (2016) FYVE1/FREE1 interacts with the PYL4 ABA receptor and mediates its delivery to the vacuolar degradation pathway. *Plant Cell* **28**: 2291–2311
- Blackmore S, Wortley AH, Skvarla JJ, Rowley JR** (2007) Pollen wall development in flowering plants. *New Phytol* **174**: 483–498
- Boutte Y, Jonsson K, McFarlane HE, Johnson E, Gendre D, Swarup R, Friml J, Samuels L, Robert S, Bhalerao RP** (2013) ECHIDNA-mediated post-Golgi trafficking of auxin carriers for differential cell elongation. *Proc Natl Acad Sci USA* **110**: 16259–16264
- Brooks J, Shaw G** (1968) Chemical structure of the exine of pollen walls and a new function for carotenoids in nature. *Nature* **219**: 532–533
- Buono RA, Paez-Valencia J, Miller ND, Goodman K, Spitzer C, Spalding EP, Otegui MS** (2016) Role of SKD1 regulators LIP5 and IST1-LIKE1 in endosomal sorting and plant development. *Plant Physiol* **171**: 251–264
- Buono RA, Leier A, Paez-Valencia J, Pennington J, Goodman K, Miller N, Ahlquist P, Marquez-Lago T, Otegui MS** (2017) ESCRT-mediated vesicle concatenation in plant endosomes. *J Cell Biol* **216**: 2167–2177
- Cai Y, Zhuang X, Gao C, Wang X, Jiang L** (2014) The *Arabidopsis* endosomal sorting complex required for transport III regulates internal vesicle formation of the prevacuolar compartment and is required for plant development. *Plant Physiol* **165**: 1328–1343.
- Cardona-López X, Cuyas L, Marín E, Rajulu C, Irigoyen ML, Gil E, Puga MI, Bligny R, Nussaume L, Geldner N, et al.** (2015) ESCRT-III-associated protein ALIX mediates high-affinity phosphate transporter trafficking to maintain phosphate homeostasis in *Arabidopsis*. *Plant Cell* **27**: 2560–2581
- Chiaruttini N, Redondo-Morata L, Colom A, Humbert F, Lenz M, Scheuring S, Roux A** (2015) Relaxation of loaded ESCRT-III spiral springs drives membrane deformation. *Cell* **163**: 866–879
- Choi H, Jin JY, Choi S, Hwang JU, Kim YY, Suh MC, Lee Y** (2011) An ABCG/WBC-type ABC transporter is essential for transport of sporopollenin precursors for exine formation in developing pollen. *Plant J* **65**: 181–193
- Choi H, Ohyama K, Kim YY, Jin JY, Lee SB, Yamaoka Y, Muranaka T, Suh MC, Fujioka S, Lee Y** (2014) The role of *Arabidopsis* ABCG9 and ABCG31 ATP binding cassette transporters in pollen fitness and the deposition of sterol glycosides on the pollen coat. *Plant Cell* **26**: 310–324
- Dettmer J, Hong-Hermesdorf A, Stierhof YD, Schumacher K** (2006) Vacuolar H⁺-ATPase activity is required for endocytic and secretory trafficking in *Arabidopsis*. *Plant Cell* **18**: 715–730
- Dimaano C, Jones CB, Hanono A, Curtiss M, Babst M** (2008) Ist1 regulates Vps4 localization and assembly. *Mol Biol Cell* **19**: 465–474
- Dou XY, Yang KZ, Zhang Y, Wang W, Liu XL, Chen LQ, Zhang XQ, Ye D** (2011) WBC27, an adenosine tri-phosphate-binding cassette protein, controls pollen wall formation and patterning in *Arabidopsis*. *J Integr Plant Biol* **53**: 74–88
- Dündar G, Shao Z, Higashitani N, Kikuta M, Izumi M, Higashitani A** (2019) Autophagy mitigates high-temperature injury in pollen development of *Arabidopsis thaliana*. *Dev Biol* **456**: 190–200
- Fan X, Yang C, Klisch D, Ferguson A, Bhaellero RP, Niu X, Wilson ZA** (2014) ECHIDNA protein impacts on male fertility in *Arabidopsis* by mediating trans-Golgi network secretory trafficking during anther and pollen development. *Plant Physiol* **164**: 1338–1349
- Frankel EB, Shankar R, Moresco JJ, Yates JR, 3rd, Volkmann N, Audhya A** (2017) Ist1 regulates ESCRT-III assembly and function during multivesicular endosome biogenesis in *Caenorhabditis elegans* embryos. *Nat Commun* **8**: 1439
- Fyfe J, Schuh AL, Edwardson JM, Audhya A** (2011) Association of ESCRT-II with VPS20 generates a curvature sensitive protein complex capable of nucleating filaments of ESCRT-III. *J Biol Chem* **286**: 34262–34270
- Gao C, Luo M, Zhao Q, Yang R, Cui Y, Zeng Y, Xia J, Jiang L** (2014) A unique plant ESCRT component, FREE1, regulates multivesicular body protein sorting and plant growth. *Curr Biol* **24**: 2556–2563
- Geldner N, Denervaud-Tendon V, Hyman DL, Mayer U, Stierhof YD, Chory J** (2009) Rapid, combinatorial analysis of membrane compartments in intact plants with a multicolor marker set. *Plant J* **59**: 169–178
- Gendre D, Oh J, Boutté Y, Best JG, Samuels L, Nilsson R, Uemura T, Marchant A, Bennett MJ, Grebe M, et al.** (2011) Conserved *Arabidopsis* ECHIDNA protein mediates trans-Golgi-network trafficking and cell elongation. *Proc Natl Acad Sci USA* **108**: 8048–8053
- Gilbert, P** (1972) Iterative methods for the three-dimensional reconstruction of an object from projections. *J Theor Biol* **36**, 105–117
- Grunewald S, Marillonnet S, Hause G, Haferkamp I, Neuhaus HE, Veß A, Hollemann T, Vogt T** (2020) The tapetal major facilitator NPF2.8 is required for accumulation of flavonol glycosides on the pollen surface in *Arabidopsis thaliana*. *Plant Cell* **32**: 1727–1748
- Haas TJ, Sliwinski MK, Martínez, MK, Preuss M, Ebine K, Ueda T, Nielsen E, Odorizzi G, Otegui MS** (2007) The *Arabidopsis* AAA ATPase SKD1 is involved in multivesicular endosome function and interacts with its positive regulator LYST-INTERACTING PROTEIN5. *Plant Cell* **19**: 1295–1312
- Hanson PI, Roth R, Lin Y, Heuser JE** (2008) Plasma membrane deformation by circular arrays of ESCRT-III protein filaments. *J Cell Biol* **180**: 389–402
- Hsieh K, Huang AHC** (2007) Tapetosomes in Brassica tapetum accumulate endoplasmic reticulum-derived flavonoids and alkanes for delivery to the pollen surface. *Plant Cell* **19**: 582–596
- Huang MD, Chen TL, Huang AH** (2013) Abundant type III lipid transfer proteins in *Arabidopsis* tapetum are secreted to the locule and become a constituent of the pollen exine. *Plant Physiol* **163**: 1218–1229
- Isono E, Katsiarimpa A, Müller IK, Anzenberger F, Stierhof Y-D, Geldner N, Chory J, Schwechheimer C** (2010) The

- deubiquitinating enzyme AMSH3 is required for intracellular trafficking and vacuole biogenesis in *Arabidopsis thaliana*. *Plant Cell* **22**: 1826–1837
- Jones CB, Ott EM, Keener JM, Curtiss M, Sandrin V, Babst M** (2012) Regulation of membrane protein degradation by starvation-response pathways. *Traffic* **13**: 468–482
- Kalinowska K, Nagel MK, Goodman K, Cuyas L, Anzenberger F, Alkhofer A, Paz-Ares J, Braun P, Rubio V, Otegui MS, et al.** (2015) *Arabidopsis* ALIX is required for the endosomal localization of the deubiquitinating enzyme AMSH3. *Proc Natl Acad Sci USA* **112**: E5543–E5551
- Katsiarimpa A, Anzenberger F, Schlager N, Neubert S, Hauser M-T, Schwechheimer C, Isono E** (2011) The *Arabidopsis* deubiquitinating enzyme AMSH3 interacts with ESCRT-III subunits and regulates their localization. *Plant Cell* **23**: 3026–3040
- Katsiarimpa A, Kalinowska K, Anzenberger F, Weis C, Ostertag M, Tsutsumi C, Schwechheimer C, Brunner F, Hüchelhoven R, Isono E** (2013) The deubiquitinating enzyme AMSH1 and the ESCRT-III subunit VPS2.1 are required for autophagic degradation in *Arabidopsis*. *Plant Cell* **25**: 2236–2252
- Katzmann DJ, Babst M, Emr SD** (2001) Ubiquitin-dependent sorting into the multivesicular body pathway requires the function of a conserved endosomal protein sorting complex, ESCRT-I. *Cell* **106**: 145–155
- Kolb C, Nagel MK, Kalinowska K, Hagmann J, Ichikawa M, Anzenberger F, Alkhofer A, Sato MH, Braun P, Isono E** (2015) FYVE1 is essential for vacuole biogenesis and intracellular trafficking in *Arabidopsis*. *Plant Physiol* **167**: 1361–1373
- Korbei B, Moulinier-Anzola J, De-Araujo L, Lucyshyn D, Retzer K, Khan MA, Luschig C** (2013) *Arabidopsis* TOL proteins act as gatekeepers for vacuolar sorting of PIN2 plasma membrane protein. *Curr Biol* **23**: 2500–2505
- Kremer JR, Mastrorarde DN, McIntosh JR** (1996) Computer visualization of three-dimensional image data using IMOD. *J Struct Biol* **116**: 71–76
- Kuromori T, Ito T, Sugimoto E, Shinozaki K** (2011) *Arabidopsis* mutant of AtABCG26, an ABC transporter gene, is defective in pollen maturation. *J Plant Physiol* **168**: 2001–2005
- Lam SK, Cai Y, Hillmer S, Robinson DG, Jiang L** (2008) SCAMPs highlight the developing cell plate during cytokinesis in tobacco BY-2 cells. *Plant Physiol* **147**: 1637–1645
- Li D-D, Xue J-S, Zhu J, Yang Z-N** (2017) Gene regulatory network for tapetum development in *Arabidopsis thaliana*. *Front Plant Sci* **8**: 1559–1559
- Li S, Yamada M, Han X, Ohler U, Benfey PN** (2016) High-resolution expression map of the *Arabidopsis* root reveals alternative splicing and lincRNA regulation. *Dev Cell* **39**: 508–522
- Lin M, Matschi S, Vasquez M, Chamness J, Kaczmar N, Baseggio M, Miller M, Stewart EL, Qiao P, Scanlon MJ, et al.** (2020) Genome-wide association study for maize leaf cuticular conductance identifies candidate genes involved in the regulation of cuticle development. *G3 (Bethesda)* **10**: 1671–1683
- Liu C, Zeng Y, Li H, Yang C, Shen W, Xu M, Xiao Z, Chen T, Li B, Cao W, et al.** (2021) A plant unique ESCRT component, FYVE4, regulates multivesicular endosome biogenesis and plant growth. *New Phytol* (in press)
- Lorraine AE, McCormick S, Estrada A, Patel K, Qin P** (2013) RNA-seq of *Arabidopsis* pollen uncovers novel transcription and alternative splicing. *Plant Physiol* **162**: 1092–1109
- Luzio JP, Hackmann Y, Dieckmann NM, Griffiths GM** (2014) The biogenesis of lysosomes and lysosome-related organelles. *Cold Spring Harb Perspect Biol* **6**: a016840
- Maity S, Caillat C, Miguet N, Sulbaran G, Effantin G, Schoehn G, Roos WH, Weissenhorn W** (2019) VPS4 triggers constriction and cleavage of ESCRT-III helical filaments. *Sci Adv* **5**: eaau7198
- Mastrorarde DN** (1997) Dual-axis tomography: an approach with alignment methods that preserve resolution. *J Struct Biol* **120**: 343–352
- McFarlane HE, Shin JJ, Bird DA, Samuels AL** (2010) *Arabidopsis* ABCG transporters, which are required for export of diverse cuticular lipids, dimerize in different combinations. *Plant Cell* **22**: 3066–3075
- McFarlane HE, Watanabe Y, Yang W, Huang Y, Ohlrogge J, Samuels AL** (2014) Golgi- and trans-Golgi network-mediated vesicle trafficking is required for wax secretion from epidermal cells. *Plant Physiol* **164**: 1250–1260
- Mierzwa BE, Chiaruttini N, Redondo-Morata L, von Filseck JM, König J, Larios J, Poser I, Müller-Reichert T, Scheuring S, Roux A, et al.** (2017) Dynamic subunit turnover in ESCRT-III assemblies is regulated by Vps4 to mediate membrane remodeling during cytokinesis. *Nat Cell Biol* **19**: 787–798
- Moulinier-Anzola J, Schwihla M, De-Araújo L, Artner C, Jörg L, Konstantinova N, Luschig C, Korbei B** (2020) TOLs function as ubiquitin receptors in the early steps of the ESCRT pathway in higher plants. *Mol Plant* **13**: 717–731
- Nickerson DP, West M, Henry R, Odorizzi G** (2010) Regulators of Vps4 ATPase activity at endosomes differentially influence the size and rate of formation of intraluminal vesicles. *Mol Biol Cell* **21**: 1023–1032
- Otegui M, Staehelin LA** (2000) Syncytial-type cell plates: a novel kind of cell plate involved in endosperm cellularization of *Arabidopsis*. *Plant Cell* **12**: 933–947
- Pacini E, Franchi GG, Hesse M** (1985) The tapetum: its form, function, and possible phylogeny in Embryophyta. *Plant Syst Evol* **149**: 155–185
- Paez Valencia J, Goodman K, Otegui MS** (2016) Endocytosis and endosomal trafficking in plants. *Ann Rev Plant Biol* **67**: 309–335
- Panikashvili D, Shi JX, Schreiber L, Aharoni A** (2011) The *Arabidopsis* ABCG13 transporter is required for flower cuticle secretion and patterning of the petal epidermis. *New Phytol* **190**: 113–124
- Panikashvili D, Shi JX, Bocobza S, Franke RB, Schreiber L, Aharoni A** (2010) The *Arabidopsis* DSO/ABCG11 transporter affects cutin metabolism in reproductive organs and suberin in roots. *Mol Plant* **3**: 563–575
- Peterson R, Slovin JP, Chen C** (2010) A simplified method for differential staining of aborted and non-aborted pollen grains. *Int J Plant Biol* **1**: 66–69
- Pfitzner A-K, Mercier V, Jiang X, Moser von Filseck J, Baum B, Šarić A, Roux A** (2020) An ESCRT-III polymerization sequence drives membrane deformation and fission. *Cell* **182**: 1140–1155
- Quilichini TD, Douglas CJ, Samuels AL** (2014a) New views of tapetum ultrastructure and pollen exine development in *Arabidopsis thaliana*. *Ann Bot* **114**: 1189–1201
- Quilichini TD, Samuels AL, Douglas CJ** (2014b) ABCG26-mediated polyketide trafficking and hydroxycinnamoyl spermidines contribute to pollen wall exine formation in *Arabidopsis*. *Plant Cell* **26**: 4483–4498
- Quilichini TD, Friedmann MC, Samuels AL, Douglas CJ** (2010) ATP-binding cassette transporter G26 is required for male fertility and pollen exine formation in *Arabidopsis*. *Plant Physiol* **154**: 678–690
- Razeq FM, Kosma DK, Rowland O, Molina I** (2014) Extracellular lipids of *Camelina sativa*: characterization of chloroform-extractable waxes from aerial and subterranean surfaces. *Phytochemistry* **106**: 188–196
- Renna L, Stefano G, Majeran W, Micalella C, Meinel T, Gigliione C, Brandizzi F** (2013) Golgi traffic and integrity depend on N-myristoyl transferase-1 in *Arabidopsis*. *Plant Cell* **25**: 1756–1773
- Renna L, Stefano G, Slabaugh E, Wormsbaecher C, Sulpizio A, Zienkiewicz K, Brandizzi F** (2018) TGNap1 is required for microtubule-dependent homeostasis of a subpopulation of the plant trans-Golgi network. *Nat Commun* **9**: 5313
- Reyes FC, Buono RA, Roschttardt H, Di Rubbo S, Yeun LH, Russinova E, Otegui MS** (2014) A novel endosomal sorting complex required for transport (ESCRT) component in *Arabidopsis*

- thaliana* controls cell expansion and development. *J Biol Chem* **289**: 4980–4988
- Rue SM, Mattei S, Saksena S, Emr SD (2008) Novel ist1-did2 complex functions at a late step in multivesicular body sorting. *Mol Biol Cell* **19**: 475–484
- Sakata T, Oshino T, Miura S, Tomabechi M, Tsunaga Y, Higashitani N, Miyazawa Y, Takahashi H, Watanabe M, Higashitani A (2010) Auxins reverse plant male sterility caused by high temperatures. *Proc Natl Acad Sci USA* **107**: 8569–8574
- Samalova M, Fricker M, Moore I (2006) Ratiometric fluorescence-imaging assays of plant membrane traffic using polyproteins. *Traffic* **7**: 1701–1723
- Sanders PM, Bui AQ, Weterings K, McIntire KN, Hsu Y-C, Lee PY, Truong MT, Beals TP, Goldberg RB (1999) Anther developmental defects in *Arabidopsis thaliana* male-sterile mutants. *Sex Plant Reprod* **11**: 297–322
- Schindelin J, Arganda-Carreras I, Frise E, Kaynig V, Longair M, Pietzsch T, Preibisch S, Rueden C, Saalfeld S, Schmid B, et al. (2012) Fiji: an open-source platform for biological-image analysis. *Nat Methods* **9**: 676–682
- Schuh AL, Audhya A (2014) The ESCRT machinery: from the plasma membrane to endosomes and back again. *Crit Rev Biochem Mol Biol* **49**: 242–261
- Segui-Simarro JM, Staehelin LA (2006) Cell cycle-dependent changes in Golgi stacks, vacuoles, clathrin-coated vesicles and multivesicular bodies in meristematic cells of *Arabidopsis thaliana*: a quantitative and spatial analysis. *Planta* **223**: 223–236
- Shahriari M, Keshavaiah C, Scheuring D, Sabovljevic A, Pimpl P, Hausler RE, Hulskamp M, Schellmann S (2010) The AAA-type ATPase AtSKD1 contributes to vacuolar maintenance of *Arabidopsis thaliana*. *Plant J* **64**: 71–85
- Shen QT, Schuh AL, Zheng Y, Quinney K, Wang L, Hanna M, Mitchell JC, Otegui MS, Ahlquist P, Cui Q, et al. (2014) Structural analysis and modeling reveals new mechanisms governing ESCRT-III spiral filament assembly. *J Cell Biol* **206**: 763–777
- Shi J, Cui M, Yang L, Kim YJ, Zhang D (2015) Genetic and biochemical mechanisms of pollen wall development. *Trends Plant Sci* **20**: 741–753
- Smyth DR, Bowman JL, Meyerowitz EM (1990) Early flower development in *Arabidopsis*. *Plant Cell* **2**: 755
- Spallek T, Beck M, Ben Khaled S, Salomon S, Bourdais G, Schellmann S, Robatzek S (2013) ESCRT-I mediates FLS2 endosomal sorting and plant immunity. *PLoS Genet* **9**: e1004035
- Spitzer C, Reyes FC, Buono R, Sliwinski MK, Haas TJ, Otegui MS (2009) The ESCRT-related CHMP1A and B proteins mediate multivesicular body sorting of auxin carriers in *Arabidopsis* and are required for plant development. *Plant Cell* **21**: 749–766
- Tan J, Davies BA, Payne JA, Benson LM, Katzmann DJ (2015) Conformational changes in the endosomal sorting complex required for transport-III subunit Ist1 lead to distinct modes of ATPase Vps4 regulation. *J Biol Chem* **290**: 30053–30065
- Valuchova S, Mikulkova P, Pecinkova J, Klimova J, Krumnikl M, Bainer P, Heckmann S, Tomancak P, Riha K (2020) Imaging plant germline differentiation within *Arabidopsis* flowers by light sheet microscopy. *eLife* **9**: e52546
- Wang F, Shang Y, Fan B, Yu JQ, Chen Z (2014) *Arabidopsis* LIP5, a positive regulator of multivesicular body biogenesis, is a critical target of pathogen-responsive MAPK cascade in plant basal defense. *PLoS Pathog* **10**: e1004243
- Wang F, Yang Y, Wang Z, Zhou J, Fan B, Chen Z (2015) A critical role of LIP5, a positive regulator of multivesicular body biogenesis, in plant responses to heat and salt stresses. *Plant Physiol* **169**: 497–511
- Wang Z, Butel N, Santos-González J, Borges F, Yi J, Martienssen RA, Martinez G, Köhler C (2020) Polymerase IV plays a crucial role in pollen development in *Capsella*. *Plant Cell* **32**: 950–966
- Webb MC, Gunning BES (1990) Embryo sac development in *Arabidopsis thaliana*. *Sex Plant Reprod* **3**: 244–256
- Wildermuth MC, Dewdney J, Wu G, Ausubel FM (2001) Isochorismate synthase is required to synthesize salicylic acid for plant defence. *Nature* **414**: 562–565
- Wollert T, Hurley JH (2010) Molecular mechanism of multivesicular body biogenesis by ESCRT complexes. *Nature* **464**: 864–869
- Wu SS, Moreau RA, Whitaker BD, Huang AH (1999) Steryl esters in the elaioplasts of the tapetum in developing Brassica anthers and their recovery on the pollen surface. *Lipids* **34**: 517–523
- Xia Z, Wei Y, Sun K, Wu J, Wang Y, Wu K (2013) The maize AAA-type protein SKD1 confers enhanced salt and drought stress tolerance in transgenic tobacco by interacting with Lyst-interacting protein 5. *PLoS One* **8**: e69787
- Xia Z, Huo Y, Wei Y, Chen Q, Xu Z, Zhang W (2016) The *Arabidopsis* LYST INTERACTING PROTEIN 5 acts in regulating abscisic acid signaling and drought response. *Front Plant Sci* **7**: 758
- Yadav V, Molina I, Ranathunge K, Castillo IQ, Rothstein SJ, Reed JW (2014) ABCG transporters are required for suberin and pollen wall extracellular barriers in *Arabidopsis*. *Plant Cell* **26**: 3569–3588
- Yim S, Khare D, Kang J, Hwang JU, Liang W, Martinoia E, Zhang D, Kang B, Lee Y (2016) Postmeiotic development of pollen surface layers requires two *Arabidopsis* ABCG-type transporters. *Plant Cell Rep* **35**: 1863–1873
- Zhang ZB, Zhu J, Gao JF, Wang C, Li H, Li H, Zhang HQ, Zhang S, Wang DM, Wang QX, et al. (2007) Transcription factor AtMYB103 is required for anther development by regulating tapetum development, callose dissolution and exine formation in *Arabidopsis*. *Plant J* **52**: 528–538
- Zhao B, Shi H, Wang W, Liu X, Gao H, Wang X, Zhang Y, Yang M, Li R, Guo Y (2016) Secretory COPII protein SEC31B is required for pollen wall development. *Plant Physiol* **172**: 1625–1642